

The RAM signaling pathway links morphology, thermotolerance, and CO₂ tolerance in the global fungal pathogen *Cryptococcus neoformans*

Benjamin J Chadwick¹, Tuyetnhu Pham¹, Xiaofeng Xie², Laura C Ristow³, Damian J Krysan^{3,4}, Xiaorong Lin^{1,2*}

¹Department of Plant Biology, University of Georgia, Athens, United States;

²Department of Microbiology, University of Georgia, Athens, United States;

³Department of Pediatrics, Carver College of Medicine, University of Iowa, Iowa City, United States; ⁴Department of Microbiology and Immunology, Carver College of

Medicine, University of Iowa, Iowa City, United States

Abstract The environmental pathogen *Cryptococcus neoformans* claims over 180,000 lives each year. Survival of this basidiomycete at host CO₂ concentrations has only recently been considered an important virulence trait. Through screening gene knockout libraries constructed in a CO₂-tolerant clinical strain, we found mutations leading to CO₂ sensitivity are enriched in pathways activated by heat stress, including calcineurin, Ras1-Cdc24, cell wall integrity, and Regulator of Ace2 and Morphogenesis (RAM). Overexpression of Cbk1, the conserved terminal kinase of the RAM pathway, partially restored defects of these mutants at host CO₂ or temperature levels. In ascomycetes such as *Saccharomyces cerevisiae* and *Candida albicans*, transcription factor Ace2 is an important target of Cbk1, activating genes responsible for cell separation. However, no Ace2 homolog or any downstream component of the RAM pathway has been identified in basidiomycetes. Through in vitro evolution and comparative genomics, we characterized mutations in suppressors of *cbk1Δ* in *C. neoformans* that partially rescued defects in CO₂ tolerance, thermotolerance, and morphology. One suppressor is the RNA translation repressor Ssd1, which is highly conserved in ascomycetes and basidiomycetes. The other is a novel ribonuclease domain-containing protein, here named *PSC1*, which is present in basidiomycetes and humans but surprisingly absent in most ascomycetes. Loss of Ssd1 in *cbk1Δ* partially restored cryptococcal ability to survive and amplify in the inhalation and intravenous murine models of cryptococcosis. Our discoveries highlight the overlapping regulation of CO₂ tolerance and thermotolerance, the essential role of the RAM pathway in cryptococcal adaptation to the host condition, and the potential importance of post-transcriptional control of virulence traits in this global pathogen.

*For correspondence:

Xiaorong.Lin@uga.edu

Competing interest: The authors declare that no competing interests exist.

Funding: See page 15

Preprinted: 14 August 2022

Received: 09 August 2022

Accepted: 22 November 2022

Published: 23 November 2022

Reviewing Editor: Arturo Casadevall, Johns Hopkins Bloomberg School of Public Health, United States

© Copyright Chadwick et al. This article is distributed under the terms of the [Creative Commons Attribution License](https://creativecommons.org/licenses/by/4.0/), which permits unrestricted use and redistribution provided that the original author and source are credited.

Editor's evaluation

This paper reports the identification of molecular determinants of CO₂ tolerance in the human fungal pathogen *Cryptococcus neoformans*. The results are important for our understanding of how the fungus adapts from the ambient atmosphere to the CO₂-enriched environment in the human host, and the findings are convincing and rely on biochemical, molecular, and genetic techniques. The results should be of interest to a broad community in the life sciences including microbiologists and infectious diseases investigators.

Introduction

There are over 278,000 cases of cryptococcal meningitis every year, causing over 180,000 deaths (*Rajasingham et al., 2017*). Cryptococcal meningitis is primarily caused by the ubiquitous environmental fungus *Cryptococcus neoformans*. Airborne spores or desiccated yeast cells of *C. neoformans* are inhaled into the lungs, where they are cleared or remain dormant until reactivation upon host immunosuppression (*Casadevall and Perfect, 1998; Zhao et al., 2019*).

Litvintseva et al. found that most environmental *Cryptococcus* isolates cannot cause fatal disease in mouse models of cryptococcosis, despite having similar genotypes and in vitro phenotypes to known virulent isolates, including thermotolerance, melanization, and capsule production (*Litvintseva and Mitchell, 2009*). *Mukaremera et al., 2019* also observed that in vitro phenotype assays for thermotolerance, capsule production, titan cell formation, or fluconazole heteroresistance could not differentiate high-virulence strains from low-virulence strains. These observations raise the possibility that other, unidentified virulence traits are important for *Cryptococcus* pathogenesis. Tolerance to host levels of CO₂ (~5% CO₂ in the host vs. ~0.04% in ambient air) is likely a significant factor separating the potentially virulent natural isolates from the non-pathogenic environmental isolates that Litvintseva et al. tested (*Krysan et al., 2019; Litvintseva and Mitchell, 2009*).

The ability to adapt to host conditions is a prerequisite for cryptococcal pathogenesis. For instance, the ability of *C. neoformans* to replicate at human body temperature ($\geq 37^\circ\text{C}$) has been extensively investigated. Many genes have been shown to be essential for thermotolerance (*Perfect, 2006; Stempinski et al., 2021; Yang et al., 2017*), including calcineurin which is currently being explored for antifungal drug development (*Gobeil et al., 2021*). By contrast, the underlying mechanisms or genes that play a role in CO₂ tolerance have yet to be identified. Here, we set out to identify CO₂-sensitive mutants and to gain the first insight into the genetic components involved in CO₂ tolerance in *C. neoformans*.

Results

CO₂ sensitivity is independent of pH

Our previous work indicates that many *C. neoformans* environmental strains are sensitive to 5% CO₂ when grown on buffered RPMI media, commonly used for mammalian cell cultures and testing antifungal susceptibility (*Krysan et al., 2019*). CO₂ at host concentrations also acts synergistically with

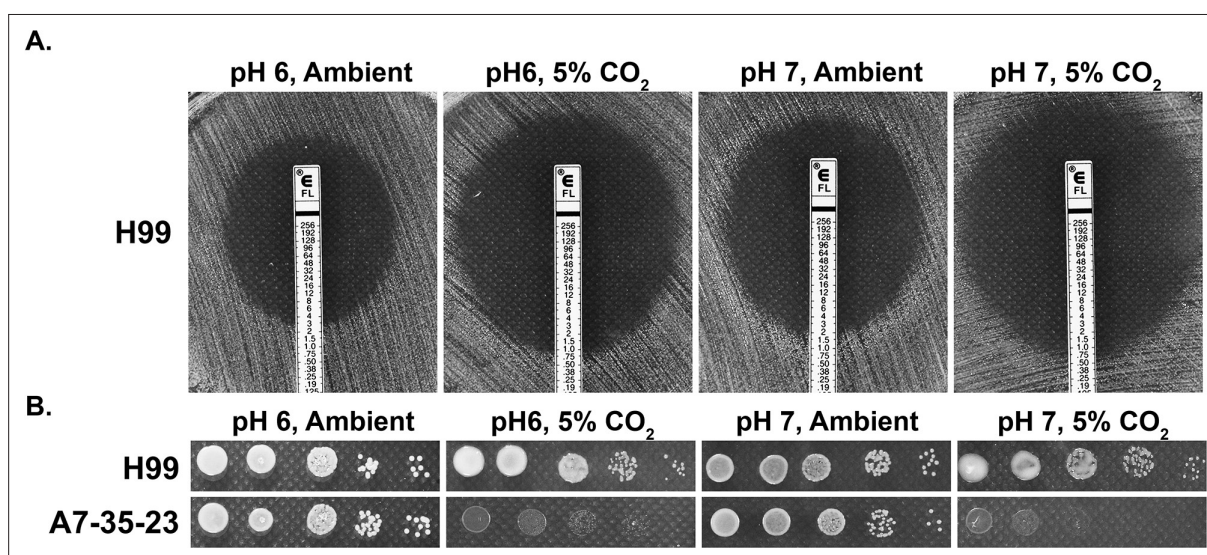


Figure 1. CO₂ sensitivity is not simply due to lowered medium pH. (A) H99 cells were plated onto RPMI solid medium buffered to either pH 6 or pH 7. Fluconazole containing E-test strips were placed onto the lawn of H99 cells, and the plates were incubated at 37°C in ambient air or in 5% CO₂. The larger the halo surrounding the E-strip, the more sensitive the cells are to fluconazole. The intercept value of the halo with the E-strip is the minimal inhibitory concentration. (B) Cells of the previously identified CO₂-tolerant H99 and CO₂-sensitive A7-35-23 were serially diluted, spotted onto RPMI media buffered to pH 6 or pH 7, and incubated at 37°C in ambient air or in 5% CO₂.

the commonly used antifungal drug fluconazole in inhibiting cryptococcal growth on buffered RPMI media. Because CO₂ lowers the pH of aqueous environments, it is possible that the CO₂ growth inhibitory effect or its synergy with fluconazole is simply due to lower medium pH. To address this question, we tested sensitivity to fluconazole of wild-type (WT) strain H99 using E-test on buffered RPMI media of either pH 6 or pH 7, with or without 5% CO₂. In this E-test, the size of halo (clearance zone) reflects fungal susceptibility to fluconazole. As shown in **Figure 1A**, clearance zones were much larger in 5% CO₂ relative to those in ambient air at both pH 6 and pH 7, indicating that CO₂ sensitizes cryptococcal susceptibility to fluconazole. Furthermore, CO₂ inhibits the growth of H99 at both pH 6 and pH 7 (smaller colony size in 5% CO₂ relative to that in ambient air). Additionally, growth of CO₂-sensitive environmental strain A7-35-23 (*Krysan et al., 2019*) was severely inhibited by 5% CO₂ at both pH 6 and pH 7 (**Figure 1B**). In general, *C. neoformans* grows better at acidic pH (can grow well

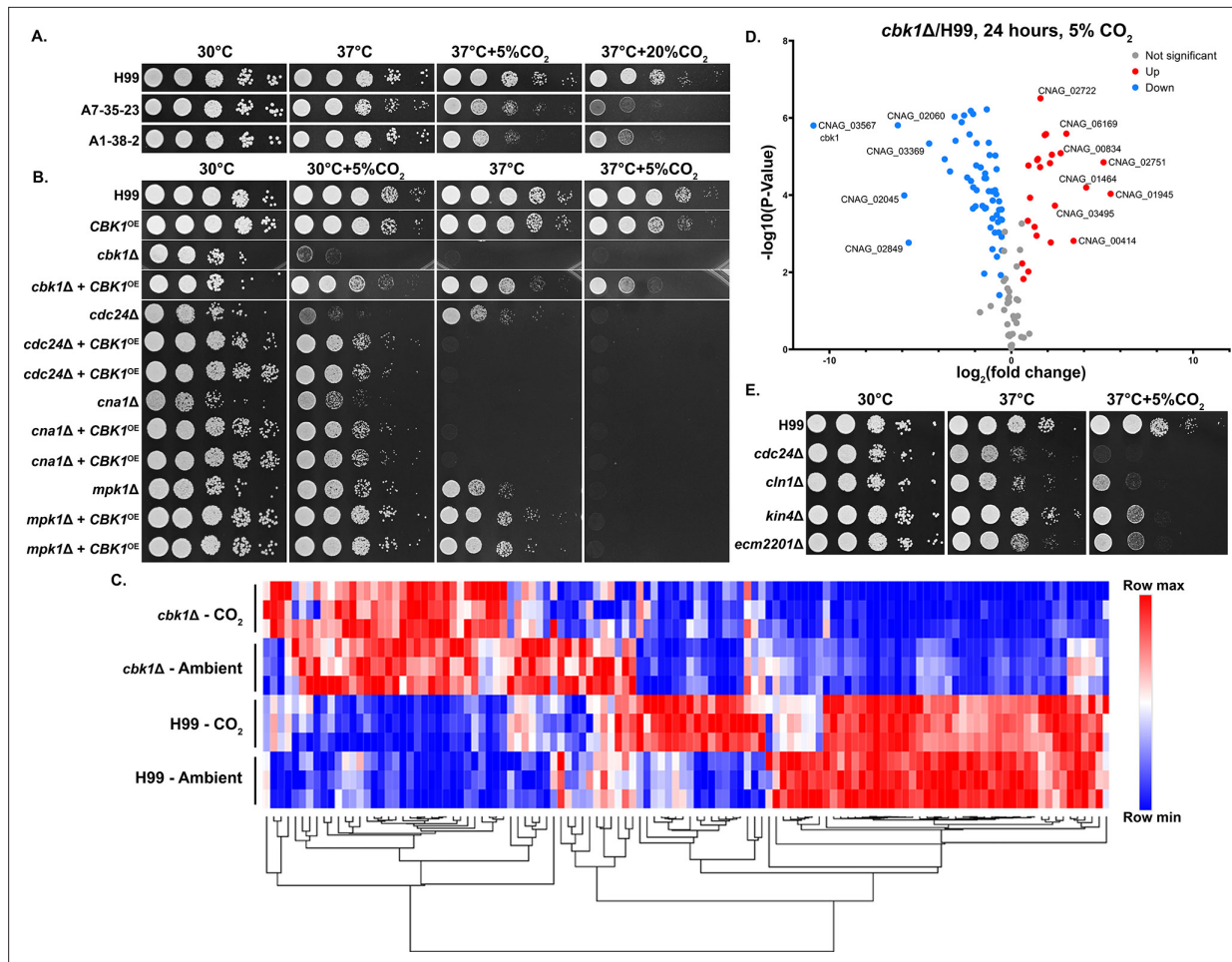


Figure 2. The Regulator of Ace2 and Morphogenesis (RAM) pathway effector kinase Cbk1 is critical for CO₂ tolerance. **(A)** The clinical reference strain H99 and environmental strains A7-35-23 and A1-38-2 were grown overnight in yeast peptone dextrose (YPD), serially diluted, and spotted onto solid YPD media plates. Photographs were taken 2 days after incubation in the indicated condition. **(B)** This serial dilution spotting assay was similarly performed for H99 and the mutants indicated. Two independent overexpression transformants for each mutant background were included as biological replicates. **(C)** Heatmap showing normalized total RNA counts of NanoString targets in H99 and *cbk1Δ* cultured at either ambient or 5% CO₂, red indicates higher and blue indicates lower transcript abundance. **(D)** Volcano plot showing significantly differentially expressed transcripts (p -value of <0.05) in the *cbk1Δ* compared to H99 in the 5% CO₂ condition. **(E)** Serial dilution spotting assay of H99 and four of the mutants found in the deletion set screening to be CO₂ sensitive which also correspond to significantly downregulated genes shown in the volcano plot.

The online version of this article includes the following figure supplement(s) for figure 2:

Figure supplement 1. The cAMP(cyclic AMP) pathway is not essential for CO₂ tolerance.

Figure supplement 2. Confirming overexpression of *CBK1*.

Figure supplement 3. Overexpression of *CDC24*, *MPK1*, or *CNA1* does not restore growth at host CO₂ or temperature levels.

in pH 3), and both A7-35-23 and H99 grew better at pH 6 than at pH 7 in ambient air (**Figure 1B**). Taken together, these results suggest that cryptococcal growth inhibition by CO₂ is not simply due to lowered pH.

Identifying genes important for CO₂ tolerance

To identify genes involved in CO₂ tolerance in *C. neoformans*, we screened gene deletion mutants constructed in the CO₂-tolerant clinical reference strain H99. For large-scale screening, we used the nutrient rich yeast peptone dextrose (YPD) medium on which *C. neoformans* grows well. Accordingly, we tested the growth of two CO₂-sensitive environmental strains and the CO₂-tolerant H99 strain in different levels of CO₂ when cultured on YPD. As expected, relative to H99, the CO₂-sensitive strains A7-35-23 and A1-38-2 grew poorly at 5% CO₂ and worse at 20% CO₂ (**Figure 2A**). Using this approach, the following deletion mutant libraries were screened at 20% CO₂ on YPD media: a set of strains previously constructed in our lab, the collections constructed by the Madhani lab, and a set generated in the Lodge Lab (**Chun and Madhani, 2010**). As some mutants are known to be temperature sensitive, we carried out the screens at 30°C rather than 37°C. From over 5000 gene knockout mutants screened (~7000 protein coding genes in the H99 genome), 96 were found to be sensitive to CO₂ by visual observation (**Supplementary file 1**). We noticed that knockout mutants for multiple pathways known to be activated by heat stress are CO₂ sensitive, including the Ras1-Cdc24 pathway, calcineurin, cell wall integrity (CWI), and Regulator of Ace2 and Morphogenesis (RAM). This finding indicates an overlapping nature of these two traits.

We were surprised by the absence of components of adenylyl cyclase-PKA (protein kinase A) pathway from the set of hits. In *Candida albicans*, the adenylyl cyclase pathway is crucial for the yeast-hypha transition in response to host levels of CO₂ (**Klengel et al., 2005**). This pathway has also been proposed to play an important role for *Cryptococcus* to sense CO₂, and the carbonic anhydrase Can1 is required for growth at low concentrations of CO₂ (**Bahn et al., 2005; Mogensen et al., 2006**). However, we found that adenylyl cyclase pathway mutants showed no growth defects at host levels CO₂, including the adenylyl cyclase mutant *cac1Δ*, the adenylyl cyclase associated protein mutant *aca1Δ*, the alpha G protein subunit mutant *gpa1Δ*, and the cAMP-dependent protein kinase mutant *pkr1Δ* (**Figure 2—figure supplement 1**). This indicates that growth defects in response to host levels of CO₂ are likely independent of bicarbonate activation of adenylyl cyclase. This is not unexpected given that bicarbonate is not a limiting factor under the high level of CO₂ used in our screen.

Because the calcineurin, Ras1-Cdc24, CWI, and RAM pathways are all activated at host temperature and were identified in our screen for CO₂-sensitive mutants, we reasoned their downstream effectors may be related or genetically interact. As the RAM pathway effector kinase mutant *cbk1Δ* showed the most severe defect in thermotolerance and CO₂ tolerance compared to the mutants of the other pathways, we first overexpressed the gene *CBK1* in the following mutants, *cdc24Δ* (Ras1-Cdc24), *mpk1Δ* (CWI), *cna1Δ* (Calcineurin), and the *cbk1Δ* mutant itself and observed their growth at host temperature and host CO₂ (**Figure 2B**). Overexpression was achieved by placing the *CBK1* open reading frame after the inducible *CTR4* promoter, which is highly activated in YPD media (**Ory et al., 2004; Wang et al., 2014; Wang et al., 2012**). The *CBK1* overexpression construct was specifically integrated into the 'safe haven' locus *SH2* (**Lin et al., 2020; Upadhyaya et al., 2017**) in each mutant strain background to avoid complications due to positional effects. We additionally confirmed overexpression of *CBK1* by RT-PCR (**Figure 2—figure supplement 2**). As expected, the growth defects of the *cbk1Δ* mutant at 37°C with and without 5% CO₂ were largely restored by *CBK1* overexpression. At 30°C, overexpression of *CBK1* restored the growth of the *mpk1Δ* mutant, the *cna1Δ* mutant, and the *cdc24Δ* mutant in the CO₂ condition. In terms of thermotolerance, overexpression of *CBK1* restored growth of *mpk1Δ* but not *cna1Δ*, while the growth defect of *cdc24Δ* at 37°C was exacerbated. *CBK1* overexpression failed to rescue growth of any of these mutants when both stressors were present (37°C+5% CO₂). We found that overexpression of *CBK1* in the WT H99 background caused a modest growth defect at 37°C+5% CO₂. Thus, the detrimental effects from *CBK1* overexpression under this growth condition may partially explain its inability to fully rescue growth of these tested CO₂-sensitive mutants. The reciprocal overexpression of *CDC24*, *MPK1*, or *CNA1* in the *cbk1Δ* mutant background did not restore growth under 37°C and/or 5% CO₂ (**Figure 2—figure supplement 3**). These results support a hypothesis that Cbk1 integrates multiple stress response pathways to regulate both CO₂ tolerance and thermotolerance.

To determine the extent of Cbk1's role in CO₂ tolerance, we conducted NanoString gene expression profiling of the WT H99 and *cbk1Δ* mutant cultured in ambient air and in 5% CO₂ at 30°C (**Figure 2C**). Transcript levels of 118 genes were measured, and those genes were chosen based on RNA sequencing results from a separate study (Ristow et al., in preparation). In that study, these genes were differentially expressed in CO₂ vs. ambient air conditions in either two CO₂-sensitive or two CO₂-tolerant natural strains (**Source data 1**). Out of these 118 CO₂-associated genes, 81 were found to be significantly differentially expressed in the *cbk1Δ* mutant in both ambient air and in 5% CO₂, indicating they are intrinsically dysregulated in the *cbk1Δ* mutant. 57/81 of these genes are downregulated and 24/81 upregulated compared to the WT H99 strain (**Figure 2D**). Interestingly, 16/57 of the downregulated genes were also hits in our deletion set screening. We picked four of these deletion mutants which showed high sensitivity in our screen, to assay their sensitivity to host CO₂ conditions by spotting assay (**Figure 2E**). Taken together, this transcriptomic profiling shows that loss of Cbk1 significantly affects the expression of CO₂-related genes.

The RAM signaling pathway is critical for normal morphology, thermotolerance, and CO₂ tolerance

The RAM pathway effector kinase Cbk1 is part of the NDR/LATS family of kinases, which is conserved from yeast to humans and affects a wide range of cellular functions including cell-cycle regulation. In *C. neoformans*, various virulence factors are impacted by deletion of *CBK1*, including urease activity and thermotolerance (**Lee et al., 2016**). Through our genetic screen for CO₂-sensitive mutants, we found that all tested *Cryptococcus* RAM pathway mutants are extremely sensitive to 5% CO₂ and high temperature, and they show no growth at 37°C+5% CO₂ (**Figure 3A**). In ascomycetes such as *Saccharomyces cerevisiae* and *C. albicans*, RAM pathway mutants are defective in cytokinesis and exhibit loss of polarity, resulting in enlarged round cells that cluster together (**Saputo et al., 2012; Figure 3—figure supplement 1A**). In contrast, though defective in cytokinesis (**Magditch et al., 2012; Walton et al., 2006**), *Cryptococcus* RAM pathway mutants are hyper-polarized and constitutively form clusters of elongated pseudohyphal cells (**Figure 3B**). Moreover, we found that while the *C. albicans* homozygous *cbk1ΔΔ* mutant exhibits a general growth defect compared to the WT control, it shows no apparent specific growth defect at 37°C with or without 5% CO₂ (**Figure 3—figure supplement 1C**). These results suggest that, although the RAM pathway is conserved in its role in cytokinesis, the effects of its downstream targets are divergent between ascomycetes and basidiomycetes.

Suppressors of the *cbk1Δ* mutant show improved growth at host conditions

In ascomycetes, Ace2 is a key downstream transcription factor of the RAM pathway (hence in the name of RAM – Regulator of Ace2 and Morphogenesis), which is important for the activation of genes responsible for cell separation as well as a large number of genes with other functions (**Mulhern et al., 2006; Wakade et al., 2020**). However, no homolog to Ace2 has been identified in *Cryptococcus* or other basidiomycetes. Furthermore, no downstream targets of the RAM pathway have been identified in any basidiomycetes. To investigate potential downstream effectors of the RAM pathway in *Cryptococcus*, we screened for spontaneous suppressor mutants of *cbk1Δ*. To do so, *cbk1Δ* mutant cells from an overnight culture in liquid YPD at 30°C were plated onto solid YPD media and incubated for 2 days at 37°C+5% CO₂. Out of >1×10⁸ cells plated and cultured under this condition that is inhibitory for growth of the original *cbk1Δ* mutant, 11 suppressor colonies were isolated for further examination and sequencing. All the suppressor isolates showed dramatically improved growth over the original *cbk1Δ* mutant at 37°C and modestly improved growth at 37°C+5% CO₂ (**Figure 4C**). Based on their distinctive phenotypes, the 11 suppressors were classified into two groups: *sup1* (2/11) and *sup2* (9/11). Shorter chains of cells in both groups indicate a partial restoration in cytokinesis (**Figure 4D**). The *sup2* group has slightly improved growth at 37°C+5% CO₂ and forms shorter chains of cells compared to the *sup1* group (**Figure 4C and D**). Besides of these observations, *sup1* and *sup2* displayed similar phenotypes in growth assays including the cryptococcal virulence traits tested, including melanin production, capsule, urease activity, and cell wall stress tolerance. (**Figure 4—figure supplement 1**). Both *sup1* and *sup2* showed no improved growth compared to the *cbk1Δ* mutant at pH 7.4 37°C+5% CO₂. This is likely due to the detrimental combination of high temperature, CO₂, and high pH, as the WT also showed significantly reduced growth in this condition. (**Figure 4—figure supplement 1A**).

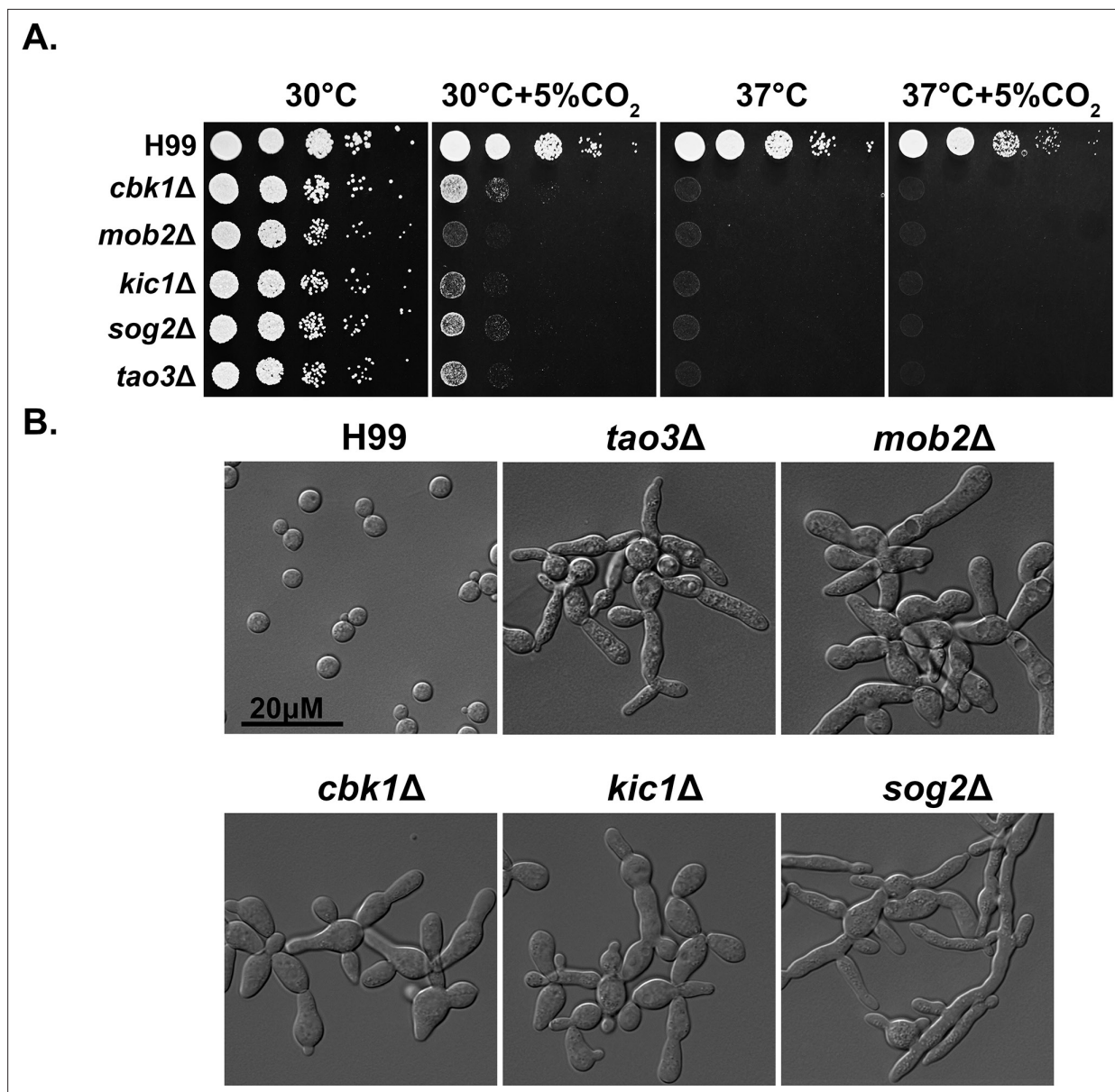


Figure 3. The Regulator of Ace2 and Morphogenesis (RAM) pathway is critical for normal morphology, thermotolerance, and CO₂ tolerance. (A) *Cryptococcus neoformans* WT H99 and RAM pathway mutants were serially diluted, spotted onto yeast peptone dextrose (YPD) medium, and incubated for 2 days at the indicated condition. (B) The cellular morphology of *C. neoformans* WT H99 and RAM pathway mutants cultured in YPD medium.

The online version of this article includes the following figure supplement(s) for figure 3:

Figure supplement 1. Conserved and divergent roles of the Regulator of Ace2 and Morphogenesis (RAM) pathway in ascomycete *Candida albicans* and basidiomycete *Cryptococcus neoformans*.

Because RAM pathway suppressor mutants were previously identified after treatment with calcineurin inhibitor FK506 and showed improved growth in FK506 and restored mating (Magditch et al., 2012), we also tested our suppressors' growth in FK506 and their ability to mate. We found that both *sup1* and *sup2* failed to restore growth of the *cbk1Δ* on media supplemented with FK506 or restore the ability to mate with the congenic strain H99a (Figure 4—figure supplement 1).

Along with the original *cbk1Δ* mutant, we sequenced the genomes of the 11 *cbk1Δ* suppressors. By comparing their genome sequences with each other and with the original *cbk1Δ* mutant, we found that both *sup1* type suppressor mutants contained a disruptive in-frame deletion at the same location

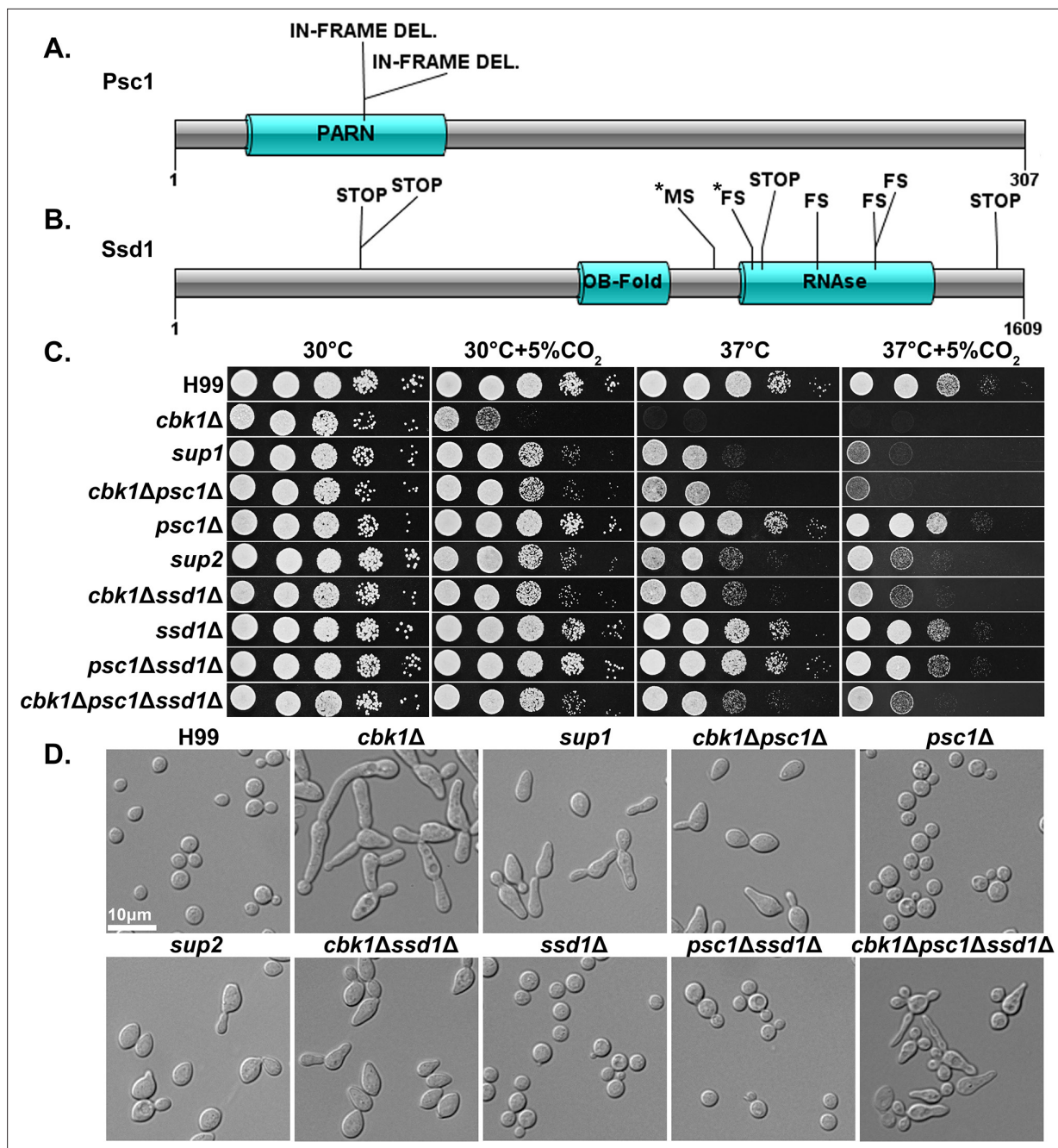


Figure 4. Natural suppressors of the Regulator of Ace2 and Morphogenesis (RAM) pathway *cbk1Δ* mutant restore multiple defects. **(A)** Protein diagram of Psc1 showing the effects and positions of suppressor mutations in the two *sup1* type natural suppressors. **(B)** Protein diagram of Ssd1 and the effects and positions of suppressor mutations in Ssd1 in the nine *sup2* type natural suppressors. STOP indicates a non-sense mutation, MS a missense mutation, and FS a frameshift mutation. Asterisks (*) indicate mutations in the same suppressor strain. **(C)** Serial dilutions of H99 and the mutant strains were spotted onto yeast peptone dextrose (YPD) agar media and incubated for 2 days in the indicated condition to observe growth. **(D)** The cellular morphology of H99 and the mutant strains in liquid YPD cultures were examined under microscope.

The online version of this article includes the following figure supplement(s) for figure 4:

Figure supplement 1. Phenotypic characterization of *cbk1Δ* suppressor mutants.

Figure supplement 2. Suppressor mutants do not restore transcript levels of NanoString targets in *cbk1Δ*.

in *CNAG_01919*, which encodes a putative Poly(A)-specific ribonuclease (PARN) domain-containing protein (**Figure 4A**). This domain was previously reported in *S. pombe* proteins (**Marasovic et al., 2013**). Interestingly, through a BLAST search of the PARN domain, we did not identify this domain in any protein in the genomes of *S. cerevisiae*, *C. albicans*, or other ascomycetes but found it in basidiomycetes and higher eukaryotes. The in-frame deletion results in a change of two amino acids within the predicted PARN domain, the only discernable domain present in this protein. We named this previously uncharacterized gene Partial Suppressor of *cbk1Δ* (*PSC1*). All nine *sup2* isolates contained loss of function or missense mutations in the gene *CNAG_03345* (**Figure 4B**), which encodes an RNA-binding protein homologous to *S. cerevisiae* Ssd1p, a known suppressor of *cbk1Δ* phenotypes in *S. cerevisiae*. ScSsd1p represses transcript translation and is negatively regulated by Cbk1p phosphorylation (**Jansen et al., 2009; Wanless et al., 2014**).

To confirm that the putative loss-of-function mutations in *SSD1* and *PSC1* are responsible for suppressing *cbk1Δ* phenotypes, we created *cbk1Δssd1Δ* and *cbk1Δpsc1Δ* double mutants together with the control single mutants *ssd1Δ* and *psc1Δ*. Indeed, relative to the *cbk1Δ* mutant, the double mutants showed reduced sensitivity to host temperature and CO₂ levels (**Figure 4C**), similar to the natural suppressor mutants. Likewise, the morphology of the double mutants resembles that of the spontaneous suppressor mutants (**Figure 4D**). The deletion of *SSD1* and *PSC1* alone in the WT background did not yield any discernable phenotype. The results confirm that loss-of-function mutations in *SSD1* and *PSC1* are responsible for partial suppression of the *cbk1Δ* mutant's growth defects observed in the isolated suppressor strains. Interestingly, *sup2* and the *cbk1Δssd1Δ* mutants both grew noticeably better than *sup1* and *cbk1Δpsc1Δ* at 37°C and 37°C+5% CO₂. To test the genetic interaction between the two suppressor genes *SSD1* and *PSC1*, we created a triple *cbk1Δpsc1Δssd1Δ* mutant and the control strain *psc1Δssd1Δ*. The *psc1Δssd1Δ* control strain did not exhibit any defect and grew similarly well to either single mutant or the WT (**Figure 4C**). The triple mutant *cbk1Δpsc1Δssd1Δ* grew similarly well as *sup2* or *cbk1Δssd1Δ* at 37°C+5% CO₂ (**Figure 4C**). However, the triple mutant displayed aberrant morphology and budding defects which are not observed in the natural suppressor mutants or the *cbk1Δssd1Δ* and *cbk1Δpsc1Δ* double mutants (**Figure 4D**). These results suggest that Psc1 and Ssd1 may function in the same pathway in regulating thermotolerance and CO₂ tolerance, but their downstream effects on cell separation and/or polarized growth may be overlapping and distinct.

To determine if the suppressor mutations restore transcript abundance of the differentially expressed genes under CO₂ in *cbk1Δ*, we compared the profiles of *cbk1Δ* to the two suppressor mutants: *sup1* and *sup2*. Overall, we found that the spontaneous suppressors do not restore transcript abundances of most differentially expressed genes in *cbk1Δ* to WT levels (**Figure 4—figure supplement 2**), suggesting that suppressors affect post-transcriptional regulation of CO₂ tolerance.

Spontaneous suppressors of *cbk1Δ* mutant show improved ability to survive and replicate in the host

RAM mutants have previously been found to be attenuated in virulence in the invertebrate wax moth larva infection model and mouse intranasal infection models (**Lee et al., 2016; Magditch et al., 2012**). Occasionally, cryptococcal strains with point mutations in RAM genes cause death of mice when revertant mutations occur, which restore the function of the RAM pathway (**Magditch et al., 2012**). As shown above and consistent with previous literature, the *cbk1Δ* mutant shows a severe growth defect at host temperature and CO₂ concentrations (**Figure 3C**). Because *sup1* and *sup2* both largely restored growth to the *cbk1Δ* mutant at 37°C but only modestly restored growth at 37°C+5% CO₂, we decided to test if, and by how much, these suppressor mutations would affect the virulence of the *cbk1Δ* mutant. We infected mice with 1×10⁴ cells of WT, *cbk1Δ*, *sup1*, or *sup2* intranasally. In this intranasal infection model, the WT H99 strain establishes lung infection first and typically disseminates to other organs including the brain by 7–10 days post-infection (DPI). Mice infected by H99 normally become morbidly ill by 3–4 weeks post-infection and have a high fungal burden in the lungs, brain, and kidney (**Chadwick and Lin, 2020; Lin et al., 2022**).

As expected, all mice infected with H99 were moribund by DPI 26 (**Figure 5A**), while those infected with the *cbk1Δ* mutant survived until the experiment was terminated at DPI 60. Surprisingly, *sup1* and *sup2* strains did not cause any mortality either. The organ fungal burden, however, revealed differences in virulence levels between these strains. At the time of euthanasia for H99-infected mice

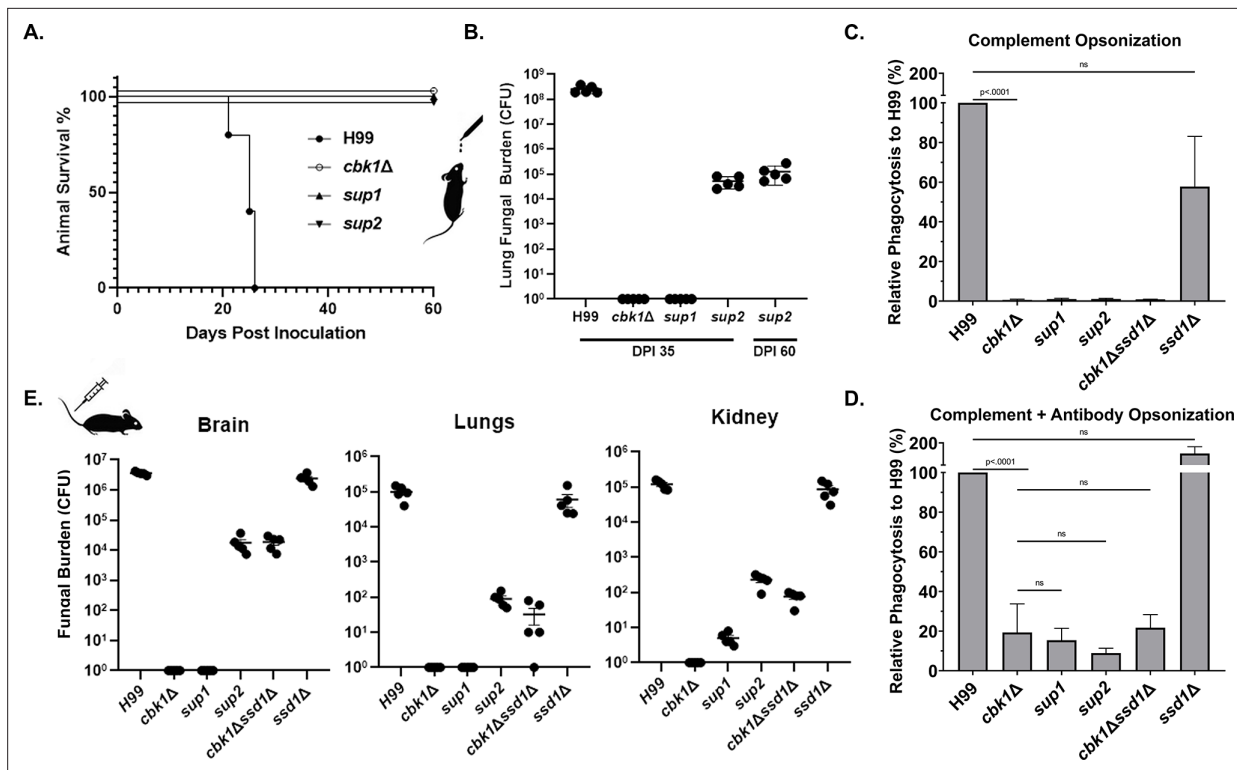


Figure 5. Suppressor mutants are partially restored for phagocytosis and can disseminate in the intravenous infection model of cryptococcosis. **(A)** Mice were infected with 1×10^4 fungal cells intranasally, and their survival was monitored for 60 days post-infection. **(B)** At day 35 post-infection (DPI 35) and at the time of termination (DPI 60), 5 out of 10 mice per group for the *cbk1Δ* mutant, *sup1* and *sup2* groups were harvested for brains, kidneys, and lungs. For H99 infected mice, they were euthanized at their clinical end point (all before DPI 26). Tissue homogenate was serially diluted and plated onto YNB(yeast nitrogen base) medium to count the colony-forming units (CFUs) to measure the fungal burden per organ. **(C)** Murine macrophage J774A.1 cells were co-incubated with 2×10^6 cryptococcal cells opsonized with serum from naïve mouse for 2 hr. Non-adherent or phagocytosed cells were washed, and cryptococcal cells were released and then serially diluted before plating onto YNB medium for measurement of CFUs. **(D)** The same as above, except opsonization, was performed with serum of mice vaccinated against cryptococcosis. **(E)** Mice were challenged with 1×10^5 cryptococcal cells intravenously. At day 5 post-infection, five mice per group were sacrificed. Brains, kidneys, and lungs of euthanized mice were dissected and homogenized. Serial dilutions were plated to count CFUs for quantification of fungal burden per organ.

(prior to DPI 26), the median fungal burden in the lungs, brains, and kidneys was 2.1×10^8 , 1.4×10^6 , and 2.4×10^4 colony-forming units (CFUs) per organ, respectively (**Figure 5B**). As expected, mice completely cleared the *cbk1Δ* mutant at DPI 35. Surprisingly, despite largely restored growth at 37°C , *sup1* was completely cleared from the mouse lungs by DPI 35, similar to the *cbk1Δ* mutant. In comparison, although *sup2* did not cause any death during the study period, it was able to replicate in the mouse lungs. The median lung fungal burden at DPI 35 was 8.2×10^4 , over eightfold higher than the original inoculum. The *sup2* strain maintained the same high lung fungal burden at DPI 60 (**Figure 5B**), indicating that it can persist in the lung tissue. The only in vitro difference observed between *sup1* and *sup2* was better growth of *sup2* at host CO_2 levels which may explain the difference in their ability to propagate and persist in the mouse lung. However, it is worth nothing that due to the complex host environment, there could be other unrecognized factors contributing to the differences in vivo.

Although the spontaneous suppressor *sup2* was able to replicate in the mouse lungs, no fungal burden was detected in the brain or the kidney at DPI 35 or 60 (no organisms were detected in any of the mice), indicating that the mutant was unable to disseminate. We considered two hypotheses: (1) inability of suppressor *sup2* to disseminate from the lungs; (2) inability of suppressor *sup2* to penetrate other organs from the blood. Because *C. neoformans* can disseminate from the lungs to other organs by a 'Trojan Horse' mechanism, where *Cryptococcus* travels within the mobile host phagocytes (**Kechichian et al., 2007; Santiago-Tirado et al., 2017**), we examined phagocytosis of the *cbk1Δ* mutant and its suppressors to test the first hypothesis. We expected that cryptococcal mutants defective in being phagocytosed by host cells might be defective in dissemination, and the *cbk1Δ* mutant

was previously found to have a poor phagocytosis index (Lin et al., 2015). Here, we co-cultured murine macrophage JA774 cells with H99, *cbk1Δ*, *sup1*, *sup2*, the double mutant *cbk1Δssd1Δ*, or the control single mutant *ssd1Δ*. Because different types of opsonization can impact phagocytosis of *C. neoformans*, opsonization was performed using either naïve mouse serum (complement mediated phagocytosis) or serum from mice vaccinated against cryptococcosis (complement+antibody mediated phagocytosis). The serum (containing antibodies) from the vaccinated mice recognizes antigens present in the capsule of cryptococcal cells (Lin et al., 2022; Zhai et al., 2015). Consistent with our previous finding, phagocytosis of the *cbk1Δ* mutant was extremely low (~1% of the WT H99 level under complement mediated phagocytosis, Figure 5C). Opsonization with serum from vaccinated mice increased phagocytosis of *cbk1Δ* and the suppressor mutants, but the phagocytosis indexes of these mutants were still only 20% or less than that of the WT (Figure 5D). In both phagocytosis experiments, the suppressor mutants or the double mutants *cbk1Δssd1Δ* and *cbk1Δpsc1Δ* mutants showed increased phagocytosis relative to the *cbk1Δ* mutant. The poor phagocytosis of the *cbk1Δ* mutant and its suppressors may contribute to their lack of dissemination from the lungs to the other organs in the inhalation infection mouse model of cryptococcosis.

To test the second hypothesis, we infected mice intravenously with H99, *cbk1Δ*, *sup1*, *sup2*, the double mutant *cbk1Δssd1Δ*, or the control single mutant *ssd1Δ*. In this intravenous infection model, the barrier of the lungs is bypassed. H99 cells disseminate to the brain and other organs within hours (O'Connor et al., 2013). Because H99 rapidly disseminates in this model, infected mice typically reach moribundity after 1 week. Therefore, we euthanized mice at DPI 5 before H99-infected mice would have become moribund. As expected, H99-infected mice showed high fungal burdens in the lungs, brains, and kidneys, with the highest fungal burden in the brain (over 10^6 CFUs; Figure 5E). The *cbk1Δ* mutant failed to disseminate in this intravenous infection model as no viable cells were recovered in any organ. Similarly, we could not recover any *sup1* cells from the lungs or the brain and only detected a few fungal cells in the kidney. In contrast, *sup2* suppressor mutants were recovered in all three organs, albeit with reduced fungal burdens (~ 10^4 CFUs in the brain and a few hundred in lungs/kidney) compared to the WT H99 control group (Figure 5E). This finding indicates that the *sup2* suppressor, once disseminated into the bloodstream, can invade other organs and replicate. Combined with the earlier observations that (1) both suppressors fully restore growth at host temperature and (2) *sup2* is slightly more CO₂ tolerant than *sup1*, the observation that only *sup2* can survive, amplify, and persist in animals implicates an importance of CO₂ tolerance in cryptococcal pathogenesis. Collectively, the

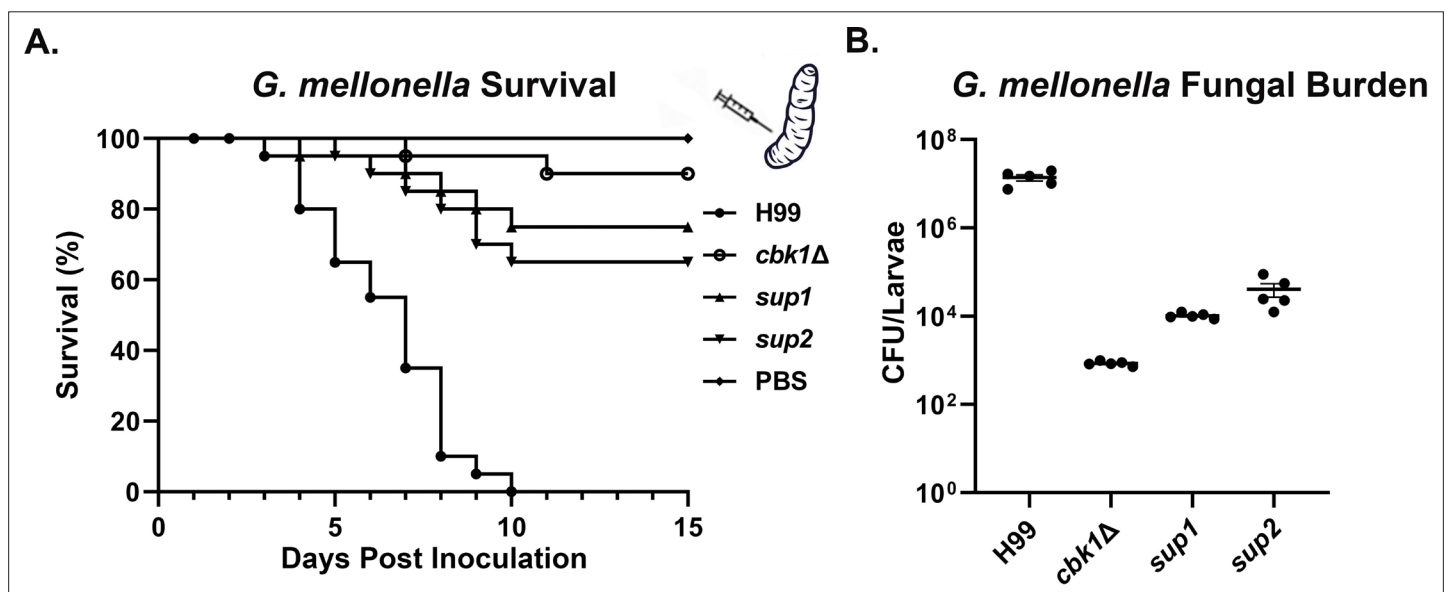


Figure 6. Suppressor mutants partially restore virulence in the *G. mellonella* model. (A) *G. mellonella* larvae were infected with 5×10^4 fungal cells of the indicated strain, and their survival was monitored for 15 days post-inoculation. The *cbk1Δ* group survival curve was not significantly different from *sup1* (p -value=0.2) and was significantly different from the *sup2* curve (p -value=0.05). (B) At day 5 post-inoculation (DPI 5), 5 out of 25 larvae per group for the H99, the *cbk1Δ* mutant, *sup1*, and *sup2* groups were homogenized, serially diluted, and plated to count the colony-forming units (CFUs) and measure the fungal burden of each larva. The fungal burden of the *sup1* and *sup2* groups was significantly higher than the *cbk1Δ* group (p -value<0.001).

results from phagocytosis, the inhalation infection model, and the intravenous infection model support the hypothesis that failure of the suppressor mutants to disseminate to other organs in the intranasal model is largely due to reduced phagocytosis and inability to escape the lungs. That said, other factors, such as increased systemic clearance by the immune system, could potentially contribute to the containment of the mutant in the lungs. Again, the *cbk1Δssd1Δ* mutant recapitulated the phenotype of the *sup2* strain in intravenous infection model and other in vitro assays, demonstrating that our observed *sup2* phenotypes are due to disruption of *SSD1*.

As mutants that are temperature sensitive have reduced virulence in the mouse model of cryptococcosis, we decided to test the virulence of these strains in the *Galleria mellonella* larvae infection model to remove temperature as a variable. We inoculated *G. mellonella* larvae with 5×10^4 cells of WT, *cbk1Δ*, *sup1*, or *sup2* and maintained the larvae at 30°C as previously described (Magditch et al., 2012). PBS buffer inoculated larvae were included as a sham control. Infected larvae (n=20 per strain) were monitored for survival over a period of 15 days post-inoculation. All 20 of the larvae inoculated with the H99 strain died between DPI 3 and DPI 10 (Figure 6A). In comparison, only 2/20 of the *cbk1Δ* mutant-infected larvae died during this period. Interestingly, 5/20 *sup1*-infected larvae and 7/20 *sup2*-infected larvae died in this experiment (Figure 6A), indicating their partially restored virulence in this larva infection model. To further confirm the observed differences between these strains in this model conducted at 30°C, we infected five larvae with 5×10^4 cells per strain and measured their fungal burden at day 5 post-inoculation. At DPI 5, the mean fungal burden of WT-infected larvae was 1.5×10^7 CFUs (Figure 6B). In comparison, the mean fungal burden for the *cbk1Δ*-infected larvae was only 8.4×10^2 CFUs, which is almost 20,000-fold lower than the WT control group and about 60-fold lower than the original inoculum, indicating that most *cbk1Δ* cells have been cleared by this time point. The mean fungal burden of *sup1*-infected larvae was 9.6×10^3 CFUs, while the mean fungal burden *sup2*-infected larvae was 2.3×10^4 CFUs (Figure 6B). These results indicate that both *sup1* and *sup2* partially rescued virulence of the *cbk1Δ* mutant and that *sup2* showed slightly better restoration of virulence compared to *sup1* in this insect model, which is independent of tolerance to mammalian body temperature.

Discussion

Detection of and adaptation to changing CO₂ levels are an important trait across biological kingdoms and may play a crucial role in the pathogenicity of fungi (Bahn and Mühlischlegel, 2006; Cummins et al., 2014; Hetherington and Raven, 2005; Krysan et al., 2019). Here, we report the identification of genes required for growth at high levels of CO₂ in the fungal pathogen *C. neoformans*. Multiple pathways important for growth at high temperature, such as the Ras1-Cdc24, CWI, Calcineurin, and RAM pathways, were found to be required for growth in high CO₂ concentrations, indicating that growth in response to host CO₂ may be intricately coordinated and co-regulated with response to host temperature. It is therefore likely that both host CO₂ and host temperature represent stressors that cryptococcal cells infecting mammalian hosts must overcome to cause disease.

Calcineurin and RAM pathways were both identified in our screen for mutants that affect cryptococcal CO₂ sensitivity. A previous study found synthetic lethality between the RAM and calcineurin pathways in *C. neoformans* but not in *S. cerevisiae* (Walton et al., 2006). This corroborates our findings of the key differences between the basidiomycete *C. neoformans* and the ascomycete yeasts. In *C. albicans*, CO₂ levels are sensed through bicarbonate or cAMP-dependent activation of adenylyl cyclase to increase hyphal growth (Du et al., 2012; Hall et al., 2010). While these pathways may also be functioning to sense CO₂ in *Cryptococcus* (Bahn et al., 2005; Mogensen et al., 2006), our results indicate that these pathways do not play a significant role in host CO₂ tolerance in *C. neoformans*. We also found that disruption of the RAM pathway effector kinase Cbk1 caused a severe growth defect at host CO₂ in *C. neoformans* but not in *C. albicans*. The vast differences between these organisms in terms of growth response to CO₂ may reflect the evolutionary distance between these species and/or the distinct niches they normally occupy. Indeed, *C. albicans* is a human commensal and has adapted to host CO₂ concentrations. *S. cerevisiae* is a powerful fermenter that thrives in conditions with high levels of CO₂. For the environmental fungus *C. neoformans*, however, the ability to grow in a CO₂-enriched condition does not appear to be strongly selected for in the natural environment, and the host level of CO₂ (~5% CO₂) is over 100-fold higher than the ambient air (~0.04% CO₂).

The RAM pathway mutants were among the most sensitive mutants to host levels of CO₂. Remarkably, the growth defects of *cbk1Δ* could be partially restored by single mutations in the genes *PSC1* or *SSD1*. While the PARN-encoding gene *PSC1* represents an uncharacterized protein, *SSD1* is a known suppressor of *cbk1Δ* phenotypes that has been extensively characterized in ascomycete yeasts to regulate the translation of numerous and diverse mRNA transcripts (Hu et al., 2018; Jansen et al., 2009; Lee et al., 2015; Li et al., 2009b; Wanless et al., 2014). Our genetic interaction analysis indicates that Psc1 likely functions in the same pathway as Ssd1. Interestingly, in *S. cerevisiae*, deletion of *SSD1* can suppress the lethality of the *cbk1Δ* mutant but not the cell separation defect, which is regulated by the transcription factor Ace2 (Kurischko et al., 2005). However, an Ace2 homolog has not been identified in *Cryptococcus* or any other basidiomycete (Lin et al., 2015). In *C. albicans*, Ssd1 plays an important role in polarized growth and hyphal initiation by negatively regulating the transcription factor Nrg1 (Lee et al., 2015). The observation that *cbk1Δpsc1Δ* and *cbk1Δssd1Δ* suppressor mutants partially rescue cell separation defects or depolarized growth suggests that *C. neoformans* may primarily utilize Ssd1/Psc1 rather than a potential Ace2 homolog to regulate cell separation or polarization. Differential regulation of target mRNA transcripts by Ssd1 and Psc1 may explain the functional divergence of the RAM pathway we observed between the basidiomycete *Cryptococcus* and the ascomycete yeasts. Our observation that the natural suppressors do not restore transcript abundances of CO₂-associated genes in *cbk1Δ* to WT levels supports a hypothesis that disruption of Ssd1 and Psc1 suppresses the *cbk1Δ* mutant's defects at a post-transcriptional level. *C. neoformans* has been demonstrated to use post-transcriptional regulation to adapt to various host stresses (Bloom et al., 2019; Kalem et al., 2021; Stovall et al., 2021). A temperature-sensitive environmental species of *Cryptococcus*, *Cryptococcus amyloletus*, fails to initiate host stress-induced translational reprogramming and is non-pathogenic (Bloom et al., 2019). Whether or not translome reprogramming is initiated in *C. neoformans* in response to host CO₂, and whether such reprogramming, if occurs, relies on Ssd1 and/or Psc1, has yet to be determined.

Materials and methods

Strains, growth conditions, and microscopy examination

Strains used in this study are listed in the key resources table. Unless stated otherwise, all *C. neoformans* cells were maintained at 30°C on YPD media or YPD + CuSO₄ (25 μM) for strains transformed with P_{CTR4}-*CBK1*. For morphological examination, all strains were examined under a Zeiss Imager M2 microscope, equipped with an AxioCam MRm camera. For spotting assays, the tested strains were grown overnight in liquid YPD medium at 30°C with shaking at 220 RPM. The cells were then adjusted to the same cell density of OD₆₀₀=1 and serially diluted 10-fold. The cell suspensions were then spotted onto YPD agar medium and incubated at the indicated condition for 2 days. CO₂ levels were controlled by a VWR CO₂ incubator or by a Pro-CO₂ controller (Biospherix, Lacona, NY, USA).

Genetic manipulation

Gene deletion constructs

To delete the gene *SSD1*, a deletion construct with a nourseothricin (NAT) resistance marker cassette with 5' and 3' homology arms to *SSD1* was used. Primers Linlab7974 (gctgcctttgctgcatctc) and Linlab7976 (ctggccgtcgttttactctcgcttctctctcta) were used to amplify the 5' arm from the H99 genome. The 3' arm was amplified from H99 with primers Linlab7977 (gtcatagctgtttctgctgattgacattgccgtcttag) and Linlab7979 (cgacctgatcaactactcgc). The NAT marker was amplified with universal primers M13F and M13R from plasmid pZP-NATcc. The three pieces were fused together by overlap PCR and amplified with nested primers Linlab7975 (acaatgagccactgcccag) and Linlab7977 (tgcgtgtt cactactgtagac). To disrupt the gene *PSC1*, a hygromycin (HYG) marker cassette was used to insert into the PARN domain. To generate the sgRNA for specific targeting to the *SSD1* locus, the *U6* promoter and sgRNA scaffold were amplified from JEC21 genomic DNA and the plasmid pDD162 using primers Linlab7980/Linlab4627 (ttgagtggggtgggtcaattaacagtataccctgcccgtg and ggctcaaagagcagatcaatg) and Linlab7981/Linlab4628 (aattgacccacccactcaagtttagagctagaatagcaagtt and cctctgacacatgcagctcc). For sgRNA targeted mutation of *PSC1*, the primers Linlab8380/Linlab4627 (tagttgttttcgcca cgcaacagtataccctgcccgtg and ggctcaaagagcagatcaatg) were used to amplify the *U6* promoter and Linlab8381/Linlab4628 (ggcgtcggcgaaaacaactagtttagagctagaatagcaagtt and cctctgacacatgcagctcc

) to amplify the sgRNA scaffold. The *U6* promoter and sgRNA scaffold were fused together by overlap PCR with primers Linlab4594/Linlab4595 (ccatcgatttgcattagaactaaaacaagca and ccgctcgagtaaaaca aaaagcaccgac) to generate the final sgRNA construct as described previously (Fan and Lin, 2018; Lin et al., 2020).

Gene overexpression constructs

The *CBK1* overexpression construct was generated by amplifying the *CBK1* open reading frame with primers Linlab7005/BC (ataggccggccatgctgatcgcccaatccag) and Linlab7006/BC (cagcatctcgtatcgt cggaag) and cloning the fragment with FseI and PacI into the pXC plasmid backbone (Wang et al., 2012), which contains the promoter of *CTR4* and neomycin resistance marker. The *CTR4* promoter is highly induced on the copper limiting YPD media. The *MPK1* overexpression construct was generated by amplifying the *MPK1* open reading frame with primers Linlab8326/BC (ataggccggccatggacaataccc ctgacac) and Linlab8327/BC (ccttaattaaggctatgataatttctgcctctcc) and cloning the fragment with FseI and AsiSI into a pUC19 plasmid backbone, containing the promoter of *GPD1* and neomycin resistance marker. The *CDC24* overexpression construct was generated by amplifying the *CDC24* open reading frame with primers Linlab6674/BC (ataggccggccatgctgtatccgggtccatctc) and Linlab6675/BC (ccttaatt aaggataaatctctctgtgggtacc) and cloning the fragment with FseI and PacI into a pUC19 plasmid backbone, containing the promoter of *CTR4* and neomycin resistance marker. The overexpression constructs were integrated into the *SH2* locus as described previously (Fan and Lin, 2018; Lin et al., 2020).

Transformation

Constructs for overexpression and deletion were transformed into *Cryptococcus* strains by the TRACE method (Fan and Lin, 2018; Lin et al., 2020), and transformants were selected on YPD medium with 100 µg/mL of NAT, 100 µg/mL of neomycin (NEO), or 200 µg/mL of HYG.

Quantitative real-time PCR

WT H99 strain along with the *cbk1Δ*, *CBK1^{OE}* strain were cultured by shaking at 220 RPM at 30°C overnight in liquid YPD medium containing 50 µM CuSO₄ to suppress the *CTR4* promoter of the *CBK1^{OE}* construct. The cultures were then diluted to OD₆₀₀=0.2 in fresh liquid YPD medium containing 50 µM BCS (bathocuproine disulfonate) to induce expression. After 5 hr of further incubation, cells were collected, flash frozen in liquid nitrogen, and lyophilized overnight. Three biological replicates per strain were used. Total RNA was isolated by using the PureLink RNA Mini Kit (Invitrogen), and first strand cDNA was synthesized using the GoScript Reverse Transcription System (Promega) following the manufacturer's instructions. The Power SYBR Green system (Invitrogen) was used for RT-PCR. The following primers were used to target *CBK1*: Linlab9217/BC (gatgctctcactcctgattcc) and Linlab8641/BC (gtacgagtctgacttcaccga). The following primers were used to target the *TEF1* housekeeping gene as an endogenous control for each sample: Linlab329/XL (cgtcaccactgaagtcaagt) and Linlab330/XL (agaagcagcctccatagg). Relative transcript level was determined using the $\Delta\Delta$ ct method as described previously. Statistical significance was determined using a Student's t-test.

NanoString RNA profiling

Overnight YPD cultures of H99, *cbk1Δ*, *cbk1Δssd1Δ*, and *cbk1Δpsc1Δ* were washed 2× in PBS and resuspended in RPMI +165 mM MOPS, pH 7.4 before quantification on an Invitrogen Countess automated cell counter. Cells were diluted to 7.5×10⁵ cells per mL in 3 mL per well in a 6-well plate. Two wells were used for each biological replicate (n=3) and condition (ambient or 5% CO₂). Plates were sealed with BreatheEasy sealing membranes (Sigma #Z380059) and incubated in a static incubator at 30°C in ambient air or 5% CO₂ for 24 hr. Cells were harvested, pelleted at 3200×g for 5 min, and the supernatant was removed. The pellets were then frozen at -80°C and lyophilized overnight. Lyophilized cells were disrupted for 45 s with 0.5 mm glass beads on an MP Biomedicals FastPrep-24 benchtop homogenizer. RNA was extracted following manufacturer instructions for the Invitrogen PureLink RNA mini-kit with on-column DNase treatment. Purified RNA was quantified on a NanoDrop OneC spectrophotometer, and a total of 100 ng per sample was combined with a custom probeset (Source data 1) from NanoString Technologies according to manufacturer instructions. Probes were hybridized at 65°C for 18 hr, then run on a NanoString nCounter SPRINT profiler according to

manufacturer instructions. Data from Reporter Code Count files were extracted with nSolver software (version 4.0), and raw counts were exported to Microsoft Excel. Internal negative controls were used to subtract background from raw counts (negative control average +2 SDs). Counts were normalized across samples by total RNA counts. Probes below background were set to a value of 1. Fold change and significance were calculated in Excel after averaging biological triplicates, using a Student t-test ($p < 0.05$). Volcano plot was generated with transformed values ($-\log[p\text{-value}]$ and $\log_2[\text{fold change}]$) in GraphPad Prism 9. Normalized total counts were used in Morpheus (<https://software.broadinstitute.org/morpheus/>) to generate a heat map, with hierarchical clustering, one minus Pearson correlation, average linkage method, and clustered according to rows and columns.

Bioinformatics

Whole genome sequencing was performed using the Illumina platform with NovaSeq 6000 at the University of California – Davis Sequencing Center, Novogene USA. A paired-end library with approximately 350 base inserts was constructed for each sample, and all libraries were multiplexed and run in one lane using a read length of 150 bases from either side.

The Illumina reads were first trimmed with Trim Galore v0.6.5 (Krueger, 2021) and then mapped to the *C. neoformans* H99 reference genome (FungiDB version 50) using the BWA-MEM algorithm of the BWA aligner v0.7.17 (Li, 2013). SAMtools v1.10 (Li et al., 2009a), Picard Tools v2.16.0 (Broad Institute, 2022), and bcftools v1.13 (Danecek et al., 2021) were used for variant calling from each sample. Variants in the suppressor strains were called with the original *cbk1Δ* mutant as a reference.

The protein diagrams of Psc1 and Ssd1 were made with the illustrator of biological sequences software package (Liu et al., 2015).

Phagocytosis assays

The authenticated mouse macrophage cell line J774A.1 (ATCC TIB-67) was acquired from the American Type Culture Collection. Before being used, normal morphology, cell adhesion, and phagocytosis activity of the cell line was confirmed. Contamination by mycoplasma was not detected. Phagocytosis assays were performed using similar procedures as we described previously (Lin et al., 2015). Briefly, 1 mL of 2×10^5 J774A.1 macrophages (MΦ) in DMEM was seeded into a 24-well plate and incubated at 37°C with 5% CO₂ for 24 hr. *Cryptococcus* strains with a starting OD₆₀₀ of 0.2 in 3 mL of liquid YPD were cultured for 16 hr. Each strain had three technical replicates. The cells were washed three times in sterile H₂O. 2×10^6 cryptococcal cells of each strain were opsonized in either 40 μL of 100% fetal bovine serum, naïve mouse serum, or mouse serum from LW10 vaccinated A/J mice (Lin et al., 2022; Zhai et al., 2015), for 30 min prior to co-incubation with MΦ. Old DMEM from MΦ was removed, and 1 mL of fresh DMEM with the opsonized *Cryptococcus* cells was added, followed by a 2 hr incubation at 37°C with 5% CO₂. The co-culture was then washed six times with warm PBS to remove non-adherent *Cryptococcus* cells. To lyse the macrophages, the cell suspensions were washed with 1 mL of cold PBS +0.01% Triton X. Serial dilutions in PBS of the cell suspensions were then plated onto YNB agar medium and allowed to grow at 30°C for 2 days to count CFUs. Statistical analyses were performed using the program Graphpad Prism 8. A two-tailed t-test was applied to determine significance. A p-value of less than 0.05 was considered significant.

G. mellonella infection model

G. mellonella larvae were purchased from Best Bait (Marblehead, OH, USA). The infection was performed as described previously (Mylonakis et al., 2005). In brief, cryptococcal strains were inoculated in 3 mL of liquid YPD medium with the initial OD₆₀₀=0.2 (approximately 10^6 cell/mL) and incubated for 15 hr at 30°C with shaking. Prior to infection, cells were washed with sterile PBS three times and adjusted to the final concentration of 1×10^7 cell/mL. 5 μL of the cell suspension (5×10^4 cells), or PBS for the control group, were injected into the last left proleg of the larvae. The proleg was cleaned with 70% ethanol prior to injection. Infected larvae were maintained at 30°C and monitored daily for survival.

Prior to fungal burden quantification, larvae were first cleaned with 70% ethanol. The larvae were cut open with sterile scissors and vortexed in a microcentrifuge tube containing 500 μL PBS and 100 μL of 0.5 mm diameter glass beads (RPI). Larval suspensions were then serially diluted in PBS and

plated onto YNB agar medium containing 50 µg/mL kanamycin and 20 µg/mL chloramphenicol and incubated at 30°C for 2 days before counting the CFUs.

Statistical analyses were performed using the program Graphpad Prism 8. The log-rank Mantel-Cox test was used to assess statistical significance of survival curves for comparison between two groups. One-way ANOVA tests were used to compare groups of three or more and for fungal burden assays.

Murine models of cryptococcosis

Intranasal infection model

Female Balb/C mice of 8–10 weeks old were purchased from the Jackson Labs (Bar Harbor, Maine). Cryptococcal strains were inoculated in 3 mL of liquid YPD medium with the initial $OD_{600}=0.2$ (approximately 10^6 cell/mL) and incubated for 15 hr at 30 °C with shaking. Prior to intranasal infection, cells were washed with sterile saline three times and adjusted to the final concentration of 2×10^5 cell/mL. Once the mice were sedated with ketamine and xylazine via intraperitoneal injection, 50 µL of the cell suspension (1×10^4 cells per mouse) were inoculated intranasally as previously described (*Lin et al., 2022; Zhai et al., 2012; Zhai et al., 2013; Zhao et al., 2020; Zhu et al., 2013*). Mice were monitored daily for disease progression. Surviving animals were euthanized at 35 or 60 DPI, and the brain, lungs, and kidneys, were dissected.

Intravenous infection model

Prior to intravenous infections, cryptococcal cells were washed with sterile saline three times and adjusted to the final concentration of 1×10^6 cell/mL. Mice were sedated with Isoflurane. 100 µL of the cell suspension (1×10^5 cells per mouse) were injected intravenously as previously described (*Zhai et al., 2012; Zhai et al., 2013; Zhao et al., 2020; Zhu et al., 2013*). After DPI 5, animals were euthanized, and the brain, lungs, and kidneys were dissected.

For fungal burden quantifications, dissected organs were homogenized in 2 mL of cold sterile PBS using an IKA-T18 homogenizer as we described previously (*Zhai et al., 2015; Zhai et al., 2012*). Tissue suspensions were serially diluted in PBS and plated onto YNB agar medium and incubated at 30°C for 2 days before counting the CFUs.

Ethical statements

This study was performed according to the guidelines of NIH and the University of Georgia Institutional Animal Care and Use Committee (IACUC). The animal models and procedures used have been approved by the IACUC (AUP protocol numbers: A2017 08–023 and A2020 06–015).

Acknowledgements

This work was supported by National Institutes of Health (<http://www.niaid.nih.gov>) (R01AI147541 to DJK and XL, and R01AI140719 to XL). The funder had no role in study design, data collection, and interpretation, or the decision to submit the work for publication. We thank all Lin lab members for their helpful suggestions. We thank Dr. Fanglin Zheng for the plasmid pFZ1, and Dr. Lukasz Kozubowski for the plasmid LKB61.

Additional information

Funding

Funder	Grant reference number	Author
National Institutes of Health	R01AI147541	Damian J Krysan Xiaorong Lin
National Institutes of Health	R01AI140719	Xiaorong Lin

The funders had no role in study design, data collection and interpretation, or the decision to submit the work for publication.

Author contributions

Benjamin J Chadwick, Conceptualization, Formal analysis, Validation, Investigation, Visualization, Methodology, Writing - original draft, Writing - review and editing; Tuyetnhu Pham, Laura C Ristow, Investigation, Visualization, Methodology; Xiaofeng Xie, Investigation, Methodology; Damian J Krysan, Resources, Funding acquisition, Project administration, Writing - review and editing; Xiaorong Lin, Conceptualization, Resources, Supervision, Funding acquisition, Investigation, Methodology, Project administration, Writing - review and editing

Author ORCIDs

Benjamin J Chadwick  <http://orcid.org/0000-0002-8244-6190>

Xiaorong Lin  <http://orcid.org/0000-0002-3390-8387>

Ethics

This study was performed according to the guidelines of NIH and the University of Georgia Institutional Animal Care and Use Committee (IACUC). The animal models and procedures used have been approved by the IACUC (AUP protocol numbers: A2017 08-023 and A2020 06-015).

Decision letter and Author response

Decision letter <https://doi.org/10.7554/eLife.82563.sa1>

Author response <https://doi.org/10.7554/eLife.82563.sa2>

Additional files**Supplementary files**

- Supplementary file 1. Hits from forward genetic screening.
- MDAR checklist
- Source data 1. NanoString probe targets.

Data availability

Sequences generated from this research has been deposited to the Sequence Read Archive (SRA) under project accession number: PRJNA791949.

The following dataset was generated:

Author(s)	Year	Dataset title	Dataset URL	Database and Identifier
Lin X	2022	Whole genome sequencing of <i>C. neoformans</i> H99 suppressor strains of the RAM pathway downstream kinase Cbk1 knockout mutant	https://www.ncbi.nlm.nih.gov/bioproject/PRJNA791949	NCBI BioProject, PRJNA791949

References

- Bahn YS**, Cox GM, Perfect JR, Heitman J. 2005. Carbonic anhydrase and CO₂ sensing during *Cryptococcus neoformans* growth, differentiation, and virulence. *Current Biology* **15**:2013–2020. DOI: <https://doi.org/10.1016/j.cub.2005.09.047>, PMID: 16303560
- Bahn Y-S**, Kojima K, Cox GM, Heitman J. 2006. A unique fungal two-component system regulates stress responses, drug sensitivity, sexual development, and virulence of *Cryptococcus neoformans*. *Molecular Biology of the Cell* **17**:3122–3135. DOI: <https://doi.org/10.1091/mbc.e06-02-0113>, PMID: 16672377
- Bahn YS**, Mühlischlegel FA. 2006. CO₂ sensing in fungi and beyond. *Current Opinion in Microbiology* **9**:572–578. DOI: <https://doi.org/10.1016/j.mib.2006.09.003>, PMID: 17045514
- Bloom ALM**, Jin RM, Leipheimer J, Bard JE, Yergeau D, Wohlfert EA, Panepinto JC. 2019. Thermotolerance in the pathogen *Cryptococcus neoformans* is linked to antigen masking via mRNA decay-dependent reprogramming. *Nature Communications* **10**:4950. DOI: <https://doi.org/10.1038/s41467-019-12907-x>, PMID: 31666517
- Broad_Institute**. 2022. Picard tools. broad institute. GitHub Repository. <http://broadinstitute.github.io/picard>
- Casadevall A**, Perfect JR. 1998. *Cryptococcus Neoformans*. ASM Press. DOI: <https://doi.org/10.1128/9781555818241>
- Chadwick BJ**, Lin X. 2020. On the history and applications of congenic strains in *Cryptococcus* research. *Pathogens* **9**:750. DOI: <https://doi.org/10.3390/pathogens9090750>, PMID: 32942570

- Chun CD**, Madhani HD. 2010. Applying genetics and molecular biology to the study of the human pathogen *Cryptococcus neoformans*. *Methods in Enzymology* **470**:797–831. DOI: [https://doi.org/10.1016/S0076-6879\(10\)70033-1](https://doi.org/10.1016/S0076-6879(10)70033-1), PMID: 20946836
- Cummins EP**, Selfridge AC, Sporn PH, Sznajder JI, Taylor CT. 2014. Carbon dioxide-sensing in organisms and its implications for human disease. *Cellular and Molecular Life Sciences* **71**:831–845. DOI: <https://doi.org/10.1007/s00018-013-1470-6>, PMID: 24045706
- Danecek P**, Bonfield JK, Liddle J, Marshall J, Ohan V, Pollard MO, Whitwham A, Keane T, McCarthy SA, Davies RM, Li H. 2021. Twelve years of samtools and bcftools. *GigaScience* **10**:giab008. DOI: <https://doi.org/10.1093/gigascience/giab008>, PMID: 33590861
- Dickinson DJ**, Ward JD, Reiner DJ, Goldstein B. 2013. Engineering the *Caenorhabditis elegans* genome using cas9-triggered homologous recombination. *Nature Methods* **10**:1028–1034. DOI: <https://doi.org/10.1038/nmeth.2641>
- Du H**, Guan G, Xie J, Cottier F, Sun Y, Jia W, Mühlischlegel FA, Huang G. 2012. The transcription factor FLO8 mediates CO₂ sensing in the human fungal pathogen *Candida albicans*. *Molecular Biology of the Cell* **23**:2692–2701. DOI: <https://doi.org/10.1091/mbc.E12-02-0094>, PMID: 22621896
- Fan Y**, Lin X. 2018. Multiple applications of a transient CRISPR-cas9 coupled with electroporation (TRACE) system in the *cryptococcus neoformans* species complex. *Genetics* **208**:1357–1372. DOI: <https://doi.org/10.1534/genetics.117.300656>, PMID: 29444806
- Gobeil SMC**, Bobay BG, Juvvadi PR, Cole DC, Heitman J, Steinbach WJ, Spicer LD. 2021. Leveraging fungal and human calcineurin-inhibitor structures. *Biophysical Data, and Dynamics To Design Selective and Nonimmunosuppressive FK506 Analogs*. *MBio* **12**:e0300021. DOI: <https://doi.org/10.1128/mBio.03000-21>
- Hall RA**, De Sordi L, Maccallum DM, Topal H, Eaton R, Bloor JW, Robinson GK, Levin LR, Buck J, Wang Y, Gow NAR, Steegborn C, Mühlischlegel FA. 2010. CO₂ acts as a signalling molecule in populations of the fungal pathogen *Candida albicans*. *PLOS Pathogens* **6**:e1001193. DOI: <https://doi.org/10.1371/journal.ppat.1001193>, PMID: 21124988
- Hetherington AM**, Raven JA. 2005. The biology of carbon dioxide. *Current Biology: CB* **15**:R406–R410. DOI: <https://doi.org/10.1016/j.cub.2005.05.042>
- Hu Z**, Xia B, Postnikoff SD, Shen ZJ, Tomoiaga AS, Harkness TA, Tyler JK. 2018. Ssd1 and gcn2 suppress global translation efficiency in replicatively aged yeast while their activation extends lifespan. *eLife* **7**:e35551. DOI: <https://doi.org/10.7554/eLife.35551>
- Jansen JM**, Wanless AG, Seidel CW, Weiss EL. 2009. Cbk1 regulation of the RNA-binding protein SSD1 integrates cell fate with translational control. *Current Biology* **19**:2114–2120. DOI: <https://doi.org/10.1016/j.cub.2009.10.071>, PMID: 19962308
- Kalem MC**, Subbiah H, Leipheimer J, Glazier VE, Panepinto JC. 2021. Puf4 mediates post-transcriptional regulation of cell wall biosynthesis and caspofungin resistance in *Cryptococcus neoformans*. *MBio* **12**:e03225–20. DOI: <https://doi.org/10.1128/mBio.03225-20>, PMID: 33436441
- Kechichian TB**, Shea J, Del Poeta M. 2007. Depletion of alveolar macrophages decreases the dissemination of a glucosylceramide-deficient mutant of *Cryptococcus neoformans* in immunodeficient mice. *Infection and Immunity* **75**:4792–4798. DOI: <https://doi.org/10.1128/IAI.00587-07>, PMID: 17664261
- Klengel T**, Liang W-J, Chaloupka J, Ruoff C, Schröppel K, Naglik JR, Eckert SE, Mogensen EG, Haynes K, Tuite MF, Levin LR, Buck J, Mühlischlegel FA. 2005. Fungal adenylyl cyclase integrates CO₂ sensing with cAMP signaling and virulence. *Current Biology* **15**:2021–2026. DOI: <https://doi.org/10.1016/j.cub.2005.10.040>, PMID: 16303561
- Kozubowski L**, Aboobakar EF, Cardenas ME, Heitman J. 2011. Calcineurin colocalizes with P-bodies and stress granules during thermal stress in *Cryptococcus neoformans*. *Eukaryotic Cell* **10**:1396–1402. DOI: <https://doi.org/10.1128/EC.05087-11>, PMID: 21724937
- Krueger F**. 2021. Trim galore. Zenodo. <https://doi.org/10.5281/zenodo.512789>
- Krysan DJ**, Zhai B, Beattie SR, Misel KM, Wellington M, Lin X. 2019. Host carbon dioxide concentration is an independent stress for *Cryptococcus neoformans* that affects virulence and antifungal susceptibility. *MBio* **10**:e01410. DOI: <https://doi.org/10.1128/mBio.01410-19>, PMID: 31266878
- Kurischko C**, Weiss G, Ottey M, Luca FC. 2005. A role for the *Saccharomyces cerevisiae* regulation of ACE2 and polarized morphogenesis signaling network in cell integrity. *Genetics* **171**:443–455. DOI: <https://doi.org/10.1534/genetics.105.042101>, PMID: 15972461
- Lee HJ**, Kim JM, Kang WK, Yang H, Kim JY. 2015. The NDR kinase Cbk1 downregulates the transcriptional repressor NRG1 through the mRNA-binding protein SSD1 in *Candida albicans*. *Eukaryotic Cell* **14**:671–683. DOI: <https://doi.org/10.1128/EC.00016-15>, PMID: 26002720
- Lee K-T**, So Y-S, Yang D-H, Jung K-W, Choi J, Lee D-G, Kwon H, Jang J, Wang LL, Cha S, Meyers GL, Jeong E, Jin J-H, Lee Y, Hong J, Bang S, Ji J-H, Park G, Byun H-J, Park SW, et al. 2016. Systematic functional analysis of kinases in the fungal pathogen *Cryptococcus neoformans*. *Nature Communications* **7**:12766. DOI: <https://doi.org/10.1038/ncomms12766>, PMID: 27677328
- Li H**, Handsaker B, Wysoker A, Fennell T, Ruan J, Homer N, Genome Project Data Processing S. 2009a. The sequence alignment/map format and samtools. *Bioinformatics* **25**:2078–2079. DOI: <https://doi.org/10.1093/bioinformatics/btp352>
- Li L**, Lu Y, Qin LX, Bar-Joseph Z, Werner-Washburne M, Breeden LL. 2009b. Budding yeast SSD1-V regulates transcript levels of many longevity genes and extends chronological life span in purified quiescent cells. *Molecular Biology of the Cell* **20**:3851–3864. DOI: <https://doi.org/10.1091/mbc.e09-04-0347>, PMID: 19570907

- Li H. 2013. Aligning Sequence Reads, Clone Sequences and Assembly Contigs with BWA-MEM. *arXiv*. <https://arxiv.org/abs/1303.3997>
- Lin J, Idnurm A, Lin X. 2015. Morphology and its underlying genetic regulation impact the interaction between *Cryptococcus neoformans* and its hosts. *Medical Mycology* **53**:493–504. DOI: <https://doi.org/10.1093/mmy/myv012>, PMID: 25841056
- Lin J, Fan Y, Lin X. 2020. Transformation of *Cryptococcus neoformans* by electroporation using a transient CRISPR-cas9 expression (TRACE) system. *Fungal Genetics and Biology* **138**:103364. DOI: <https://doi.org/10.1016/j.fgb.2020.103364>, PMID: 32142753
- Lin J, Pham T, Hipsher K, Glueck N, Fan Y, Lin X, Chowdhary A. 2022. Immunoprotection against cryptococcosis offered by *znf2* depends on capsule and the hyphal morphology. *MBio* **0**:e02785-21. DOI: <https://doi.org/10.1128/mbio.02785-21>
- Litvintseva AP, Mitchell TG. 2009. Most environmental isolates of *Cryptococcus neoformans* var. *grubii* (serotype A) are not lethal for mice. *Infection and Immunity* **77**:3188–3195. DOI: <https://doi.org/10.1128/IAI.00296-09>, PMID: 19487475
- Liu W, Xie Y, Ma J, Luo X, Nie P, Zuo Z, Lahrmann U, Zhao Q, Zheng Y, Zhao Y, Xue Y, Ren J. 2015. Ibs: an illustrator for the presentation and visualization of biological sequences. *Bioinformatics* **31**:3359–3361. DOI: <https://doi.org/10.1093/bioinformatics/btv362>, PMID: 26069263
- Magditch DA, Liu TB, Xue C, Idnurm A. 2012. Dna mutations mediate microevolution between host-adapted forms of the pathogenic fungus *Cryptococcus neoformans*. *PLOS Pathogens* **8**:e1002936. DOI: <https://doi.org/10.1371/journal.ppat.1002936>, PMID: 23055925
- Marasovic M, Zocco M, Halic M. 2013. Argonaute and triman generate dicer-independent priRNAs and mature siRNAs to initiate heterochromatin formation. *Molecular Cell* **52**:173–183. DOI: <https://doi.org/10.1016/j.molcel.2013.08.046>, PMID: 24095277
- Mogensen EG, Janbon G, Chaloupka J, Steegborn C, Fu MS, Moyrand F, Klengel T, Pearson DS, Geeves MA, Buck J, Levin LR, Mühlischlegel FA. 2006. *Cryptococcus neoformans* senses CO₂ through the carbonic anhydrase *can2* and the adenylyl cyclase *Cac1*. *Eukaryotic Cell* **5**:103–111. DOI: <https://doi.org/10.1128/EC.5.1.103-111.2006>, PMID: 16400172
- Mukaremera L, McDonald TR, Nielsen JN, Molenaar CJ, Akampurira A, Schutz C, Taseera K, Muzoora C, Meintjes G, Meya DB, Boulware DR, Nielsen K. 2019. The mouse inhalation model of *Cryptococcus neoformans* infection recapitulates strain virulence in humans and shows that closely related strains can possess differential virulence. *Infection and Immunity* **87**:e00046-19. DOI: <https://doi.org/10.1128/IAI.00046-19>, PMID: 30833336
- Mulhern SM, Logue ME, Butler G. 2006. *Candida albicans* transcription factor ACE2 regulates metabolism and is required for filamentation in hypoxic conditions. *Eukaryotic Cell* **5**:2001–2013. DOI: <https://doi.org/10.1128/EC.00155-06>, PMID: 16998073
- Mylonakis E, Moreno R, El Khoury JB, Idnurm A, Heitman J, Calderwood SB, Ausubel FM, Diener A. 2005. *Galleria mellonella* as a model system to study *Cryptococcus neoformans* pathogenesis. *Infection and Immunity* **73**:3842–3850. DOI: <https://doi.org/10.1128/IAI.73.7.3842-3850.2005>, PMID: 15972469
- Nielsen K, Cox GM, Wang P, Toffaletti DL, Perfect JR, Heitman J. 2003. Sexual cycle of *Cryptococcus neoformans* var. *grubii* and virulence of congenic α and β isolates. *Infection and Immunity* **71**:4831–4841. DOI: <https://doi.org/10.1128/IAI.71.9.4831-4841.2003>, PMID: 12933823
- O'Connor L, Livermore J, Sharp AD, Goodwin J, Gregson L, Howard SJ, Felton TW, Schwartz JA, Neely MN, Harrison TS, Perfect JR, Hope WW. 2013. Pharmacodynamics of liposomal amphotericin B and flucytosine for cryptococcal meningoencephalitis: safe and effective regimens for immunocompromised patients. *The Journal of Infectious Diseases* **208**:351–361. DOI: <https://doi.org/10.1093/infdis/jit164>, PMID: 23599314
- Ory JJ, Griffith CL, Doering TL. 2004. An efficiently regulated promoter system for *Cryptococcus neoformans* utilizing the CTR4 promoter. *Yeast* **21**:919–926. DOI: <https://doi.org/10.1002/yea.1139>, PMID: 15334556
- Perfect JR. 2006. *Cryptococcus neoformans*: the yeast that likes it hot. *FEMS Yeast Research* **6**:463–468. DOI: <https://doi.org/10.1111/j.1567-1364.2006.00051.x>, PMID: 16696642
- Rajasingham R, Smith RM, Park BJ, Jarvis JN, Govender NP, Chiller TM, Denning DW, Loyse A, Boulware DR. 2017. Global burden of disease of HIV-associated cryptococcal meningitis: an updated analysis. *The Lancet Infectious Diseases* **17**:873–881. DOI: [https://doi.org/10.1016/S1473-3099\(17\)30243-8](https://doi.org/10.1016/S1473-3099(17)30243-8), PMID: 28483415
- Santiago-Tirado FH, Onken MD, Cooper JA, Klein RS, Doering TL. 2017. Trojan horse transit contributes to blood-brain barrier crossing of a eukaryotic pathogen. *MBio* **8**:e02183-16. DOI: <https://doi.org/10.1128/mbio.02183-16>, PMID: 28143979
- Saputo S, Chabrier-Rosello Y, Luca FC, Kumar A, Krysan DJ. 2012. The ram network in pathogenic fungi. *Eukaryotic Cell* **11**:708–717. DOI: <https://doi.org/10.1128/EC.00044-12>, PMID: 22544903
- Stempinski PR, Zielinski JM, Dbouk NH, Huey ES, McCormack EC, Rubin AM, Chandrasekaran S, Kozubowski L. 2021. Genetic contribution to high temperature tolerance in *Cryptococcus neoformans*. *Genetics* **217**:1–15. DOI: <https://doi.org/10.1093/genetics/iyaa009>, PMID: 33683363
- Stovall AK, Knowles CM, Kalem MC, Panepinto JC. 2021. A conserved *gcn2-gcn4* axis links methionine utilization and the oxidative stress response in *Cryptococcus neoformans*. *Frontiers in Fungal Biology* **2**:640678. DOI: <https://doi.org/10.3389/ffunb.2021.640678>, PMID: 34622246
- Upadhyaya R, Lam WC, Maybruck BT, Donlin MJ, Chang AL, Kayode S, Ormerod KL, Fraser JA, Doering TL, Lodge JK. 2017. A fluorogenic *C. neoformans* reporter strain with a robust expression of m-cherry expressed from a safe Haven site in the genome. *Fungal Genetics and Biology* **108**:13–25. DOI: <https://doi.org/10.1016/j.fgb.2017.08.008>, PMID: 28870457

- Wakade RS**, Ristow LC, Stamnes MA, Kumar A, Krysan DJ. 2020. The Ndr/LATS kinase Cbk1 regulates a specific subset of ACE2 functions and suppresses the hypha-to-yeast transition in *Candida albicans*. *MBio* **11**:e01900-20. DOI: <https://doi.org/10.1128/mBio.01900-20>, PMID: 32817109
- Walton FJ**, Heitman J, Idnurm A. 2006. Conserved elements of the ram signaling pathway establish cell polarity in the basidiomycete *Cryptococcus neoformans* in a divergent fashion from other fungi. *Molecular Biology of the Cell* **17**:3768–3780. DOI: <https://doi.org/10.1091/mbc.e06-02-0125>, PMID: 16775005
- Wang L**, Zhai B, Lin X. 2012. The link between morphotype transition and virulence in *Cryptococcus neoformans*. *PLOS Pathogens* **8**:e1002765. DOI: <https://doi.org/10.1371/journal.ppat.1002765>, PMID: 22737071
- Wang L**, Tian X, Gyawali R, Upadhyay S, Foyle D, Wang G, Cai JJ, Lin X. 2014. Morphotype transition and sexual reproduction are genetically associated in a ubiquitous environmental pathogen. *PLOS Pathogens* **10**:e1004185. DOI: <https://doi.org/10.1371/journal.ppat.1004185>, PMID: 24901238
- Wanless AG**, Lin Y, Weiss EL. 2014. Cell morphogenesis proteins are translationally controlled through UTRs by the NDR/LATS target SSD1. *PLOS ONE* **9**:e85212. DOI: <https://doi.org/10.1371/journal.pone.0085212>, PMID: 24465507
- Yang D-H**, Jung K-W, Bang S, Lee J-W, Song M-H, Floyd-Averette A, Festa RA, Ianiri G, Idnurm A, Thiele DJ, Heitman J, Bahn Y-S. 2017. Rewiring of signaling networks modulating thermotolerance in the human pathogen *Cryptococcus neoformans*. *Genetics* **205**:201–219. DOI: <https://doi.org/10.1534/genetics.116.190595>, PMID: 27866167
- Zhai B.**, Wu C, Wang L, Sachs MS, Lin X. 2012. The antidepressant sertraline provides a promising therapeutic option for neurotropic cryptococcal infections. *Antimicrobial Agents and Chemotherapy* **56**:3758–3766. DOI: <https://doi.org/10.1128/AAC.00212-12>, PMID: 22508310
- Zhai B**, Zhu P, Foyle D, Upadhyay S, Idnurm A, Lin X. 2013. Congenic strains of the filamentous form of *Cryptococcus neoformans* for studies of fungal morphogenesis and virulence. *Infection and Immunity* **81**:2626–2637. DOI: <https://doi.org/10.1128/IAI.00259-13>, PMID: 23670559
- Zhai B**, Wozniak KL, Masso-Silva J, Upadhyay S, Hole C, Rivera A, Wormley FL, Lin X. 2015. Development of protective inflammation and cell-mediated immunity against *Cryptococcus neoformans* after exposure to hyphal mutants. *MBio* **6**:e01433-15. DOI: <https://doi.org/10.1128/mBio.01433-15>, PMID: 26443458
- Zhao Y**, Lin J, Fan Y, Lin X. 2019. Life cycle of *Cryptococcus neoformans*. *Annual Review of Microbiology* **73**:120210. DOI: <https://doi.org/10.1146/annurev-micro-020518-120210>
- Zhao Y**, Wang Y, Upadhyay S, Xue C, Lin X. 2020. Activation of meiotic genes mediates ploidy reduction during cryptococcal infection. *Current Biology: CB* **30**:1387–1396. DOI: <https://doi.org/10.1016/j.cub.2020.01.081>
- Zhu P**, Zhai B, Lin X, Idnurm A. 2013. Congenic strains for genetic analysis of virulence traits in *Cryptococcus gattii*. *Infection and Immunity* **81**:2616–2625. DOI: <https://doi.org/10.1128/IAI.00018-13>, PMID: 23670558

Appendix 1

Appendix 1—key resources table

Reagent type (species) or resource	Designation	Source or reference	Identifiers	Additional information
Genetic reagent (<i>Cryptococcus neoformans</i> KN99 α , mata)	WT strain: H99	Nielsen et al., 2003		
Genetic reagent (<i>C. neoformans</i> KN99 α , mata)	WT strain: H99 α	Nielsen et al., 2003		
Genetic reagent (<i>C. neoformans</i> KN99 α , mata)	cbk1 Δ	Walton et al., 2006	FJW9	H99alpha, CBK1::NAT
Genetic reagent (<i>C. neoformans</i> KN99 α , mata)	mob2 Δ	Walton et al., 2006	FJW10	H99alpha, MOB2::NAT
Genetic reagent (<i>C. neoformans</i> KN99 α , mata)	kic1 Δ	Walton et al., 2006	FJW8	H99alpha, KIC1::NAT
Genetic reagent (<i>C. neoformans</i> KN99 α , mata)	tao3 Δ	Walton et al., 2006	A136	MATalpha, TAO3:: NAT
Genetic reagent (<i>C. neoformans</i> KN99 α , mata)	sog2 Δ	Walton et al., 2006	A131	MATalpha, SOG2:: NAT
Genetic Reagent (<i>Candida albicans</i> , SN250)	SN250	Wakade et al., 2020	SN250	HIS-, LEU-, ARG-
Genetic Reagent (<i>C. albicans</i> , SN250)	cbk1 $\Delta\Delta$	Wakade et al., 2020	$\Delta\Delta$ cbk1	SN250, $\Delta\Delta$ cbk1: HIS-, LEU-, ARG-
Genetic reagent (<i>C. neoformans</i> KN99 α , mata)	cna1 Δ	FGSC deletion set Plate 46 Well E12	cna1 Δ	H99alpha CNA1::NAT
Genetic reagent (<i>C. neoformans</i> KN99 α , mata)	cdc24 Δ	FGSC deletion set Plate 33 Well C4	cdc24 Δ	H99alpha, CDC24::NAT
Genetic reagent (<i>C. neoformans</i> KN99 α , mata)	mpk1 Δ	FGSC deletion set Plate 11 Well A5	mpk1 Δ	H99alpha, MPK1::NAT
Genetic reagent (<i>C. neoformans</i> KN99 α , mata)	CBK1 ^{OE}	This study.	BC1449	H99alpha, P _{CTR4} -CBK1-mCherry- NEO'
Genetic reagent (<i>C. neoformans</i> KN99 α , mata)	cdc24 Δ , CBK1 ^{OE}	This study.	BC1281	H99alpha, CDC24::NAT, P _{CTR4} -CBK1-mCherry- NEO'
Genetic reagent (<i>C. neoformans</i> KN99 α , mata)	cdc24 Δ , CBK1 ^{OE}	This study.	BC1282	H99alpha, CDC24::NAT, P _{CTR4} -CBK1-mCherry- NEO'
Genetic reagent (<i>C. neoformans</i> KN99 α , mata)	cna1 Δ , CBK1 ^{OE}	This study.	BC1283	H99alpha, CNA1::NAT, P _{CTR4} -CBK1-mCherry- NEO'
Genetic reagent (<i>C. neoformans</i> KN99 α , mata)	cna1 Δ , CBK1 ^{OE}	This study.	BC1284	H99alpha, CNA1::NAT, P _{CTR4} -CBK1-mCherry- NEO'
Genetic reagent (<i>C. neoformans</i> KN99 α , mata)	mpk1 Δ , CBK1 ^{OE}	This study.	BC1285	H99alpha, MPK1::NAT, P _{CTR4} -CBK1-mCherry- NEO'

Appendix 1 Continued on next page

Appendix 1 Continued

Reagent type (species) or resource	Designation	Source or reference	Identifiers	Additional information
Genetic reagent (<i>C. neoformans</i> KN99 α , mata)	<i>mpk1</i> Δ , <i>CBK1</i> ^{OE}	This study.	BC1286	H99alpha, <i>MPK1::NAT</i> , <i>P_{CTR4}-CBK1-mCherry-NEO'</i>
Genetic reagent (<i>C. neoformans</i> KN99 α , mata)	<i>cdc24</i> Δ , <i>CDC24</i> ^{OE}	This study.	BC650	H99alpha, <i>CDC24::NAT</i> , <i>P_{CTR4}-mNeonGreen-CDC24-NEO'</i>
Genetic reagent (<i>C. neoformans</i> KN99 α , mata)	<i>cbk1</i> Δ , <i>CBK1</i> ^{OE}	This study.	BC669	H99alpha, <i>CBK1::NAT</i> , <i>P_{CTR4}-CBK1-mCherry-NEO'</i>
Genetic reagent (<i>C. neoformans</i> KN99 α , mata)	<i>mpk1</i> Δ , <i>MPK1</i> ^{OE}	This study.	BC1356	H99alpha, <i>MPK1::NAT</i> , <i>P_{GPD1}-mNeonGreen-MPK1-NEO'</i>
Genetic reagent (<i>C. neoformans</i> KN99 α , mata)	<i>cna1</i> Δ , <i>CNA1</i> ^{OE}	Kozubowski et al., 2011	LK214	H99a, <i>CNA1::NEO'</i> , <i>P_{HIS}-GFP-CNA1-NAT'</i>
Genetic reagent (<i>C. neoformans</i> KN99 α , mata)	<i>cbk1</i> Δ , <i>CDC24</i> ^{OE}	This study.	BC1357	H99alpha, <i>CBK1::NAT</i> , <i>P_{CTR4}-mNeonGreen-CDC24-NEO'</i>
Genetic reagent (<i>C. neoformans</i> KN99 α , mata)	<i>cbk1</i> Δ , <i>MPK1</i> ^{OE}	This study.	BC1358	H99alpha, <i>CBK1::NAT</i> , <i>P_{GPD1}-mNeonGreen-MPK1-NEO'</i>
Genetic reagent (<i>C. neoformans</i> KN99 α , mata)	<i>cbk1</i> Δ , <i>CNA1</i> ^{OE}	This study.	BC1359	H99alpha, <i>CBK1::NAT</i> , <i>P_{HIS}-GFP-CNA1-NAT'</i>
Genetic reagent (<i>C. neoformans</i> KN99 α , mata)	<i>sup1</i>	This study.	BC1068	H99alpha, <i>CBK1::NAT,SUP1</i>
Genetic reagent (<i>C. neoformans</i> KN99 α , mata)	<i>sup2</i>	This study.	BC1076	H99alpha, <i>CBK1::NAT,SUP2</i>
Genetic reagent (<i>C. neoformans</i> KN99 α , mata)	<i>cbk1</i> Δ <i>ssd1</i> Δ	This study.	BC1239	H99alpha, <i>CBK1::NAT</i> , <i>SSD1::NEO'</i>
Genetic reagent (<i>C. neoformans</i> KN99 α , mata)	<i>ssd1</i> Δ	This study.	BC1241	H99alpha, <i>SSD1::NEO'</i>
Genetic reagent (<i>C. neoformans</i> KN99 α , mata)	<i>cbk1</i> Δ <i>psc1</i> Δ	This study.	BC1369	H99alpha, <i>CBK1::NAT</i> , <i>PSC1::HYG'</i>
Genetic reagent (<i>C. neoformans</i> KN99 α , mata)	<i>psc1</i> Δ	This study.	BC1393	H99alpha, <i>PSC1::HYG'</i>
Genetic reagent (<i>C. neoformans</i> KN99 α , mata)	<i>cac1</i> Δ	Bahn et al., 2006	YSB42	H99alpha, <i>CAC1::NAT</i> STM#159
Genetic reagent (<i>C. neoformans</i> KN99 α , mata)	<i>aca1</i> Δ	FGSC deletion set Plate 32 Well H6	<i>aca1</i> Δ	H99alpha, <i>ACA1::NAT</i>
Genetic reagent (<i>C. neoformans</i> KN99 α , mata)	<i>pkr1</i> Δ	FGSC deletion set Plate 33 Well H7	<i>pkr1</i> Δ	H99alpha, <i>PKR1::NAT</i>
Genetic reagent (<i>C. neoformans</i> KN99 α , mata)	<i>pde1</i> Δ	FGSC deletion set Plate 10 Well A12	<i>pde1</i> Δ	H99alpha, <i>PDR1::NAT</i>

Appendix 1 Continued on next page

Appendix 1 Continued

Reagent type (species) or resource	Designation	Source or reference	Identifiers	Additional information
Genetic reagent (<i>C. neoformans</i> KN99 α , mata)	<i>pde2</i> Δ	FGSC deletion set Plate 11 Well H7	<i>pde2</i> Δ	H99alpha, PDR2::NAT ^r
Genetic reagent (<i>C. neoformans</i> KN99 α , mata)	<i>gpa1</i> Δ	Bahn et al., 2005	YSB83	H99alpha, GPA1::NAT ^r STM#5
Genetic reagent (<i>C. neoformans</i> KN99 α , mata)	<i>cln1</i> Δ	This study.	BZ36	H99alpha, CLN1::NAT ^r
Genetic reagent (<i>C. neoformans</i> KN99 α , mata)	<i>ecm2201</i> Δ	FGSC deletion set Plate 2 Well A10	<i>ecm2201</i> Δ	H99alpha, ECM2201::NAT ^r
Genetic reagent (<i>C. neoformans</i> KN99 α , mata)	<i>kin4</i> Δ	Bahn Kinase Deletion Set Plate 4 Well G8 (Lee et al., 2016)	<i>kin4</i> Δ	H99alpha, KIN4::NAT ^r
Recombinant DNA reagent	pPZP-NATcc	Dickinson et al., 2013	pPZP-NATcc	
Recombinant DNA reagent	pDD162	Walton et al., 2006	pDD162	
Recombinant DNA reagent	pFZ1-CDC24	This study.	P _{CTR4-2'} -mNeonGreen-CDC24(H99)-NEO ^r	
Recombinant DNA reagent	pXC-CBK1-mCh	This study.	P _{CTR4-2'} -CDC24(H99)-mCherry-NEO ^r	
Recombinant DNA reagent	LKB61	Kozubowski et al., 2011	P _{GPD1} -mCherry-CNA1-HYG ^r	
Recombinant DNA reagent	pUC19-MPK1-mNG	This study.	P _{GPD1} -MPK1-mNeonGreen-NEO ^r	
Cell line (<i>Mus. Musculus</i> , macrophage cell line J774A.1)	J774A.1	American Type Culture Collection	ATCC TIB-67	
Chemical Compound and drug	Hygromycin	Research Products International	Cat. NO.: H75000	
Chemical Compound and drug	G418	Research Products International	Cat. NO.: G64000	
Chemical Compound and drug	Nourseothricin	Jena Bioscience	Cat. NO.: AB-102-25 G	
Software and algorithm	Graphpad Prism 9	Graphpad		
Software and algorithm	nSolver software version 4.0	NanoString Technologies		
Software and algorithm	Trim Galore v0.6.5	Krueger, 2021		
Software and algorithm	BWA aligner v0.7.17	Li, 2013		
Software and algorithm	SAMtools v1.10	Li et al., 2009a		
Software and algorithm	Picard Tools v2.16.0	Broad Institute, 2022		
Software and algorithm	bcftools v1.13	Danecek et al., 2021		
Software and algorithm	Illustrator of biological sequences (IBS)	Liu et al., 2015		